The SPIRE Analogue Signal Chain and Photometer Detector Data Processing Pipeline

Document Number: SPIRE-UCF-DOC-002890

Issue 3

9 October 2007

Matt Griffin

Contents

1. Introduction

The purpose of this note is to describe the propagation of the SPIRE science data signals from the detectors through to the digitised samples transmitted to the ground, and to outline the methods by which the measured detector voltages are to be converted to astronomical signals.

Section 2 contains a list of the symbols used in the document.

Section 3 describes the analogue signal chains for both the photometer and FTS, and is largely based on information in the *DCU Design Document* (*DCU DD*) [1]. It concludes with a description of how the Photometer and Spectrometer Data Timeline (PDT and SDT) products (bolometer voltage, current, and resistance) can be derived from the telemetry data. This section applies both to the photometer and FTS pipelines, the only differences being in the values of various parameters and in the form of some of the transfer functions. Subsequent stages of the two pipelines will have some common features, but will be different in many respects. The FTS pipeline following the derivation of the Spectrometer Detector Timeline (SDT) products is described in detail in [2].

Section 4 presents an outline of the detector data pipeline for the photometer. Two options are considered:

(i) the "model-based" pipeline, which uses physical models of the bolometers and their operating temperatures, involves calculation of the absorbed radiant power as an intermediate step in the derivation of the astronomical signals, and is in principle capable of correcting for both thermal variations and detector non-linearity;

(ii) the "empirical" pipeline, in which the detector voltages are used directly to derive the astronomical signals, and which requires empirically-based corrections to be made in order to correct for thermal effects and non-linear response.

The advantages and disadvantages of these two options are discussed, and it is concluded that the empirical pipeline should be implemented in the first instance.

2. List of symbols

Symbol	Definition
A_{Tel}	Telescope effective collecting area
B	Calibration constant combining RSRF, telescope area and overall efficiency
C_{H}	Capacitance of the harness between the detector and JFET input
$\mathbf{C_{elec}}$	Electrical crosstalk matrix
$\mathbf{C_{opt}}$	Optical crosstalk matrix
DATA	16-bit ADC output value corresponding to a detector voltage value
e_{ij}	Coefficient of electrical crosstalk matrix linking output of detector i to detector j
f_{b}	Bias modulation frequency
G_{d}	Bolometer dynamic thermal conductance ($\mathrm{d}W/\mathrm{d}T$)
$G_{\mathrm{d\text{-}300mK}}$	G_{d} at 300 mK
G_{LIA}	Gain of signal chain between JFET output and low-pass filter output
G_{tot}	Total gain of analogue signal chain from JFET output to the ADC
$H_{\mathrm{BPF}}(w_{\mathrm{b}})$	Transfer function of the DCU band-pass filter
$H_{\mathrm{Demod}}(f)$	Square-wave demodulator transfer function as a function of input phase difference
$H_{\mathrm{H}}(w_{\mathrm{b}})$	Transfer function of the harness between the detector and JFET input
$H_{\mathrm{JFET}}(w_{\mathrm{b}})$	Transfer function of the JFET
$H_{\mathrm{LPF}}(w_{\mathrm{b}})$	Transfer function of the DCU low-pass filter

H_o	Bandpass filter peak gain
K	Constant of proportionality relating source flux density to absorbed detector power
K_1	Coefficient of 2nd-order correction to linear relationship between source flux density and V_S
$i_b(t)$	Bias current as a function of time
I_b	Bias current amplitude
$I_{d\text{-}RMS}$	RMS value of detector current
j	$\sqrt{-1}$
f_{samp}	Detector sampling frequency
n_{samp}	Number of detector samples per BSM position in chopped mode
o_{ij}	Coefficient of optical crosstalk matrix linking output of detector i to detector j
OFFSET	4-bit offset used to generate offset voltage to be subtracted from LPF output voltage
P	Electrical power dissipated in the bolometer
$Q(t)$	Total radiant power absorbed by a bolometer as a function of time
Q_B	Background power absorbed by a bolometer
Q_C	Radiant power from the astronomical calibration source absorbed by a bolometer
Q_S	Radiant power from the astronomical source absorbed by a bolometer
R_d	Detector resistance
R_L	Total load resistance
R_S	Bolometer resistance parameter
$R(n)$	Relative Spectral Response Function of a photometer band
$S_S(n)$	Astronomical source in-beam flux density at frequency n
$S_C(n)$	Astronomical calibration source in-beam flux density at frequency n
t	Time
t_{wait}	Delay between issue of BSM move command and first detector sample for the new position
T_b	Period of bias waveform (= $1/f_b$) [not to be confused with temperature]
T_g	Bolometer material band-gap temperature
T_o	Bolometer bath temperature
$v_b(t)$	Bias voltage as a function of time
V_b	Bias voltage amplitude
$v_d(t)$	Voltage across detector as a function of time
V_{ADC}	Voltage input to the ADC, from which *DATA* is derived
V_{BPF}	Amplitude of voltage at the band-pass filter input
V_d	Amplitude of voltage across detector
$V_{d\text{-}RMS}$	RMS value of voltage across detector
V_{Demod}	DC voltage amplitude at demodulator output
V_{JFET}	Amplitude of the voltage at the JFET output
$V_{JFET\text{-}RMS}$	RMS voltage at the JFET output
V_{LPF}	Amplitude of voltage at the low-pass filter input
V_o	RMS detector voltage at the operating point in the absence of any astronomical signal
V_{Offset}	Voltage level generated by the DAC from *OFFSET*, and subtracted from the LPF output voltage
V_S	Decrease in RMS detector voltage at the operating point due to the astronomical signal
W	Total power dissipated in the bolometer
a_C	Astronomical calibration source power law spectral index
a_S	Astronomical source power law spectral index
b	Bolometer thermal conductivity power law index
$\Delta V_{JFET\text{-}RMS}$(1 bit)	Change in RMS voltage at the JFET output that corresponds to a 1-bit change in the value of *DATA*
Δf	Phase difference between demodulator reference and input signals
f	Bolometer temperature normalised to the bath temperature

$h(n)$	Overall efficiency for coupling between flux density at the telescope aperture and power absorbed by a detector
t_B , t'_B	Bandpass filter time constant parameters
n	FIR/submm radiation frequency
n_o	Radiation frequency characterising a photometer band, and for which the astronomical flux density is quoted
t_H	Time constant defined by the JFET harness capacitance and the parallel combination of the detector and load resistances
w_b	Angular frequency of detector bias voltage
w_S	Angular frequency of detector signal modulation

3. The SPIRE on-board electronics chain

3.1 Bolometer bias and readout

Figure 1 shows the essential features of the bolometer bias and readout electronics used in SPIRE. The bolometer is biased (heated, by applied electrical power P, to its optimum operating temperature of around $1.3T_o$) by a sinusoidal excitation at angular frequency w_b, corresponding to a frequency, $f_b = w_b/2\pi$, of around 100 Hz. The sinusoidal bias excitation is applied via the two load resistors each with resistance $R_L/2$ (~ 10 MΩ each). The resistance of a SPIRE detector at the operating point, R_d, is typically 3 MΩ. The bias excitation is much faster than the thermal time constant, so that bias itself does not produce a temperature modulation, and the impedance of the detector at the bias frequency is also purely resistive. This AC biasing is preferred over DC bias as it up-converts the signal information to the bias frequency, getting well above the $1/f$ noise knee of the JFET readout amplifiers. With this arrangement, because of the inherently low $1/f$ noise of the bolometers, the $1/f$ noise knee of the system can be very low (less than 0.1 Hz).

The detector signals are fed to the JFET source followers, and the JFET outputs are connected via the long cryoharness to the warm electronics.

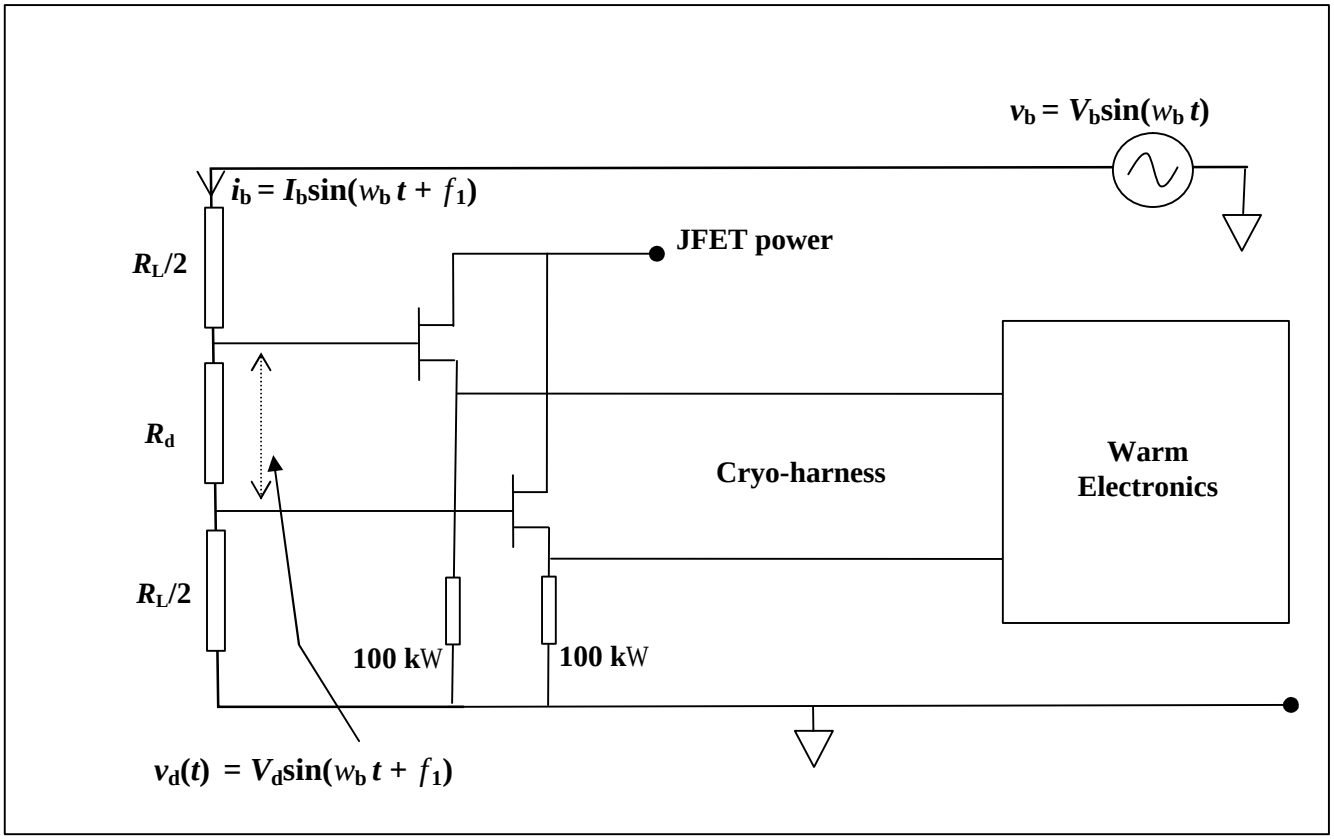

Figure 1: SPIRE bolometer bias and readout circuit

Let the applied AC bias voltage be

$$v_b(t) = V_b \sin(w_b t), \tag{1}$$

producing a bias current, flowing through the load resistor and the detector, given by

$$i_b(t) = I_b \sin(w_b t + f_1), \tag{2}$$

where f_1 is some phase difference between output of the bias generator in the warm electronics and the bolometer current.

The corresponding AC voltage across the detector is,

$$v_d(t) = V_d \sin(w_b t + f_1), \tag{3}$$

where $V_d = I_b R_d$.

The operating point on the load curve corresponds to the RMS values of the detector voltage and current:

$$V_{d\text{-RMS}} = \frac{V_d}{\sqrt{2}} \qquad I_{b\text{-RMS}} = \frac{I_d}{\sqrt{2}} \qquad P = V_{d\text{-RMS}} I_{b\text{-RMS}}. \tag{4}$$

The amplitude of bolometer signal, V_d , will vary if the radiant power on the detector is being modulated (for instance by chopping or telescope scanning in the case of the photometer or movement of the scan mirror in the case of the spectrometer. For a radiant signal modulated at frequency w_S ($<< w_b$) we will represent the corresponding signal amplitude as $V_d(w_S)$.

3.2 Block diagram of the analogue electronics chain

A model of the complete SPIRE signal chain is shown in Figure 2. The detector signals are de-modulated by individual lock-in amplifiers (LIAs). An LIA comprises a bandpass filter and a square wave demodulator, followed by a low-pass filter. The output of the LIA is nominally a DC voltage proportional to the RMS value of the voltage at the bolometer output. The LIA outputs are multiplexed and sampled for telemetry to the ground. In order to achieve the necessary 20-bit sampling using only a 16-bit ADC, an offset subtraction scheme is implemented. The functions and characteristics of each element of the chain are described in the following sections.

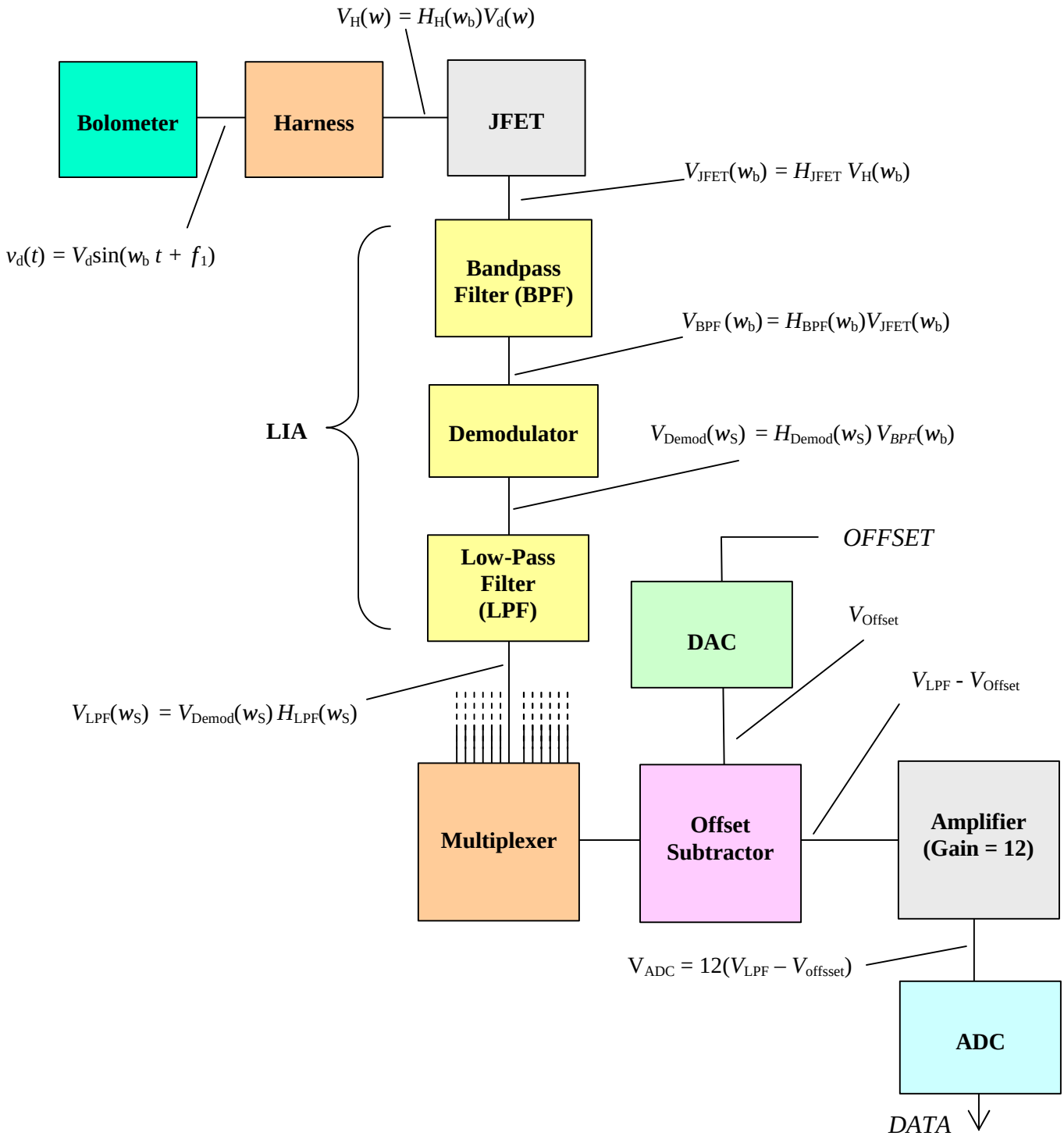

Figure 2: SPIRE bolometer signal chain

3.3 Detector – JFET harness

The detector signals are fed to JFETs located outside the SPIRE FPU. The JFET input capacitance plus the stray capacitance of the harness between the detector and the JFET forms an *RC* filter with the parallel combination of the detector and the load resistance. This results in a some attenuation and phase change of the signal. Let the total capacitance (harness + JFET input capacitance) be C_H. The harness transfer function is represented as

$$H_H(w_b) = \frac{1}{1 + jw_b t_H}\ , \tag{5}$$

where $j = \sqrt{-1}$,

and $$t_H = \left[\frac{R_L R_d}{R_L + R_d}\right] C_H . \tag{6}$$

The magnitude of $H_H(w_b)$ is $$\left|H_H(w_b)\right| = \frac{1}{\left[1 + (w_b t_H)^2\right]^{1/2}} .$$

The values of C_H currently adopted are 50 pF for the photometer detectors and 20 pF for the spectrometer detectors. For R_L = 20 MΩ, R_d = 3 MΩ, and $w_b = 2p(130)$ rad s^{-1}, the corresponding value of $\left|H_H(w_b)\right|$, is 0.994 with a phase of about 6^o.

3.4 JFETs

The output of the JFET source followers reproduce their input voltages, with a small attenuation, and – importantly – with a much lower output impedance than the detector. This allows the next stage of amplification to be located in the warm electronics with negligible attenuation due to capacitance of the several metres of cable in between.

The JFETs have a transfer function, H_{JFET}, which we take to be uniform over the range of bias frequencies used in SPIRE. The magnitude of H_{JFET} is slightly less than unity, and we also assume that it is the same for both JFETs in that pair. Currently, a representative value of H_{JFET} = 0.96 is adopted for all JFETs. It is planned to measure the gain explicitly for each channel, and a calibration table of gains will be produced.

The RMS voltage at the JFET output is

$$V_{JFET-RMS}(w_b) = \left|H_H(w_b) H_{JFET}\right| V_{d-RMS} \quad . \tag{7}$$

The signal from the JFETs is demodulated by the LIA, which has three stages:

(i) a band-pass filter/amplifier to remove the DC component and amplify the signal;
(ii) a square-wave synchronous demodulator which rectifies the signal;
(iii) a low-pass filter which produces a low-frequency output proportional to V_d.

3.5 Band-pass filter

The transfer function of the SPIRE bandpass filter is given by

$$H_{BPF}(w_b) = H_o\left[\frac{jw_b t_B}{1 + jw_b t_B + (jw_b)^2 t'_B t_B}\right], \qquad (8)$$

where H_o = 262.8 for the photometer detectors and 114.4 for the spectrometer detectors, t_B = 4.7 ms, and $t'_B = 1.25 \times 10^{-4}$ s for the photometer and 6.68×10^{-5} s for the spectrometer (*DCU DD* p. 36; p. 54).

The magnitude of H_{BPF} as a function of bias frequency is plotted in Figure 3 for both the photometer and spectrometer. It is designed to be fairly flat across the range of bias frequencies that are expected to be used.

For the nominal photometer and spectrometer bias frequencies, we have:

Photometer (w_b = 130 Hz): $|H_{BPF}| = 259.61$;

Spectrometer (w_b = 190 Hz): $|H_{BPF}| = 113.81$.

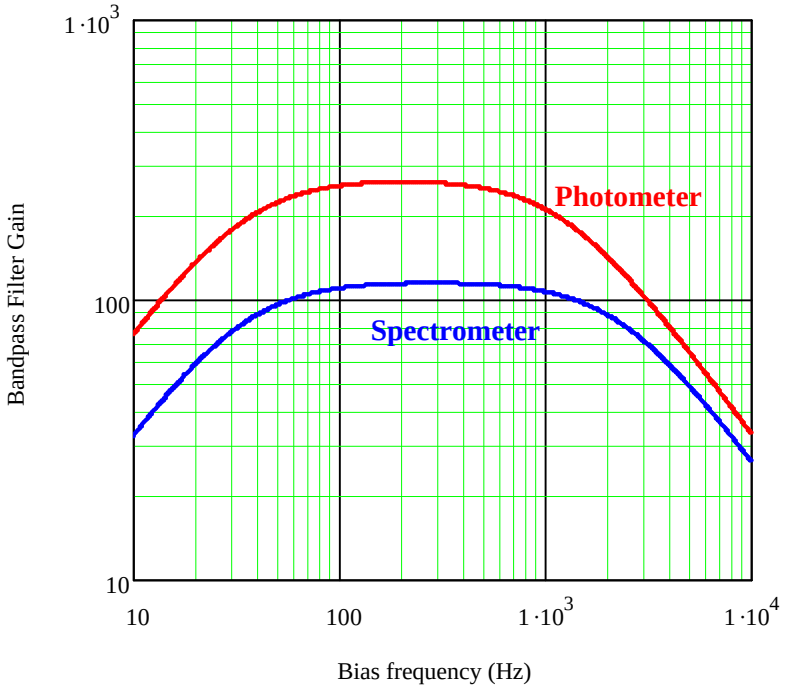

Figure 3: Magnitude of band-pass filter gain vs. bias frequency

3.6 Square-wave demodulator

The demodulator multiplies the alternating input signal by a square wave reference voltage which is ideally in phase with the input signal, such that the multiplication factor is +1 during the positive half-cycle of the input and -1 during the negative half-cycle. It then functions as a perfect rectifier. Under these conditions, the DC or low-frequency component of the demodulator output is just the mean value of a rectified sine wave: $(2/p)V_{BPF} = (0.637)V_{BPF}$, where V_{BPF} is the amplitude of the input. But the output will be less than this if the phase of the reference is not perfectly matched to that of the input. The (frequency-independent) transfer function, as a function of phase difference Δf, is given by

$$H_{\text{Demod}}(?\,f) = \left[\frac{2}{p}\right]\cos(?\,f)\,, \tag{9}$$

which is plotted in Figure 4.

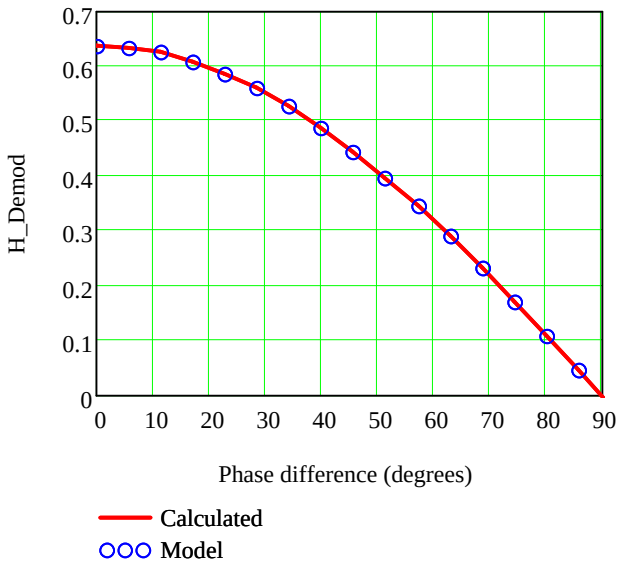

Figure 4: Demodulator gain vs. phase input difference. The red curve shows the gain as explicitly calculated by direct integration of the rectified waveform, and the blue dots correspond to H_{Demod} as given by equation (9)

For the case of near zero w_S (slowly varying radiant power), the demodulator output is a DC voltage related to the amplitude of the JFET output voltage by

$$V_{\text{Demod}}(w_b, f) = H_{\text{BPF}}(w_b) H_{\text{Demod}}(?\,f)\, V_{\text{JFET}}\ , \tag{10}$$

so

$$V_{\text{Demod}}(w_b, f) = \sqrt{2} H_{\text{BPF}}(w_b) H_{\text{Demod}}(?\,f)\, V_{\text{JFET-RMS}}\ . \tag{11}$$

If V_d is varying at angular frequency w_S (<< w_b) due to detector radiant power modulation, then V_{Demod} will also vary accordingly.

The phase difference is dictated largely by the bolometer-JFET harness time constant, t_H. In setting up the LIAs, the phase of the LIA reference can be adjusted for each array, so as to correct for the phase difference f_1 in equation (2) and hence make Δf equal to zero. In flight, it will be adjusted to make Δf = 0 for the nominal operating condition (telescope background; pointing at blank sky). There will be a slight degree of non-optimal phase due to the spread in detector impedances across the array. Furthermore, since the detector impedance varies with radiant loading, a component of phase mismatch will also arise when looking at bright sources. Let the nominal bolometer resistance be $R_{\text{d-nom}}$ (this will be the resistance when the telescope views dark sky). If the resistance changes significantly from this value (due for instance to a strong signal power), then a phase shift will be introduced:

$$Df = \tan^{-1}(w_b t_{\text{H-nom}}) - \tan^{-1}(w_b t_{\text{H}}) = \tan^{-1}\left(w_b\left[\frac{R_L R_{\text{d-nom}}}{R_L + R_{\text{d-mom}}}\right]C_H\right) - \tan^{-1}\left(w_b\left[\frac{R_L R_d}{R_L + R_d}\right]C_H\right). \quad (12)$$

This phase difference will be small, and, as can be seen from Figure 4, its effect on the demodulator transfer function is also small. Nevertheless, it can be taken into account in the procedure for calculating the bolometer resistance (see Section 3.15).

3.7 Low-pass filter

The low pass filter following the demodulator is designed to reject all higher-frequency components from the demodulator output, passing just the DC or slowly varying voltage directly proportional to the amplitude of the detector voltage. If the radiant signal on the detector is constant, then it will be just a DC component. If the radiation is modulated at angular frequency w_S (within the filter passband) then there will be a corresponding LPF output at angular frequency w_S.

For the photometer, the low-pass filters are implemented as 4-pole Bessel filters, with transfer function given by (*DCU DD* p.40):

$$H_{\text{LPF-P}}(w_S) = \left[\frac{1.93}{1 + jw_S(42.6\times10^{-3}) + (jw_S)^2(5\times10^{-4})}\right]\left[\frac{1}{1 + jw_S(25\times10^{-3}) + (jw_S)^2(4\times10^{-4})}\right] \times\left[\frac{1}{1 + jw_S(10^{-3})}\right]. \quad (13)$$

and for the spectrometer, 6-pole Bessel filters are used, with transfer function given by (*DCU DD* p.53)

$$H_{\text{LPF-S}}(w_S) = \left[\frac{2.86}{1 + jw_S(7.85\times10^{-3}) + (jw_S)^2(1.6\times10^{-5})}\right]\left[\frac{1}{1 + jw_S(3.25\times10^{-3}) + (jw_S)^2(1.09\times10^{-5})}\right] \times\left[\frac{1}{1 + jw_S(6.26\times10^{-3}) + (jw_S)^2(1.47\times10^{-5})}\right]\left[\frac{1}{1 + jw_S(10^{-4})}\right]. \quad (14)$$

The magnitudes of these are plotted vs. detector modulation angular frequency (w_S) in Figure 5 on linear and logarithmic scales.

For a bolometer channel with low w_S (no or very slow modulation of the radiant power), the DC gain of the LPF applies:

$|H_{\text{LPF-P}}(0)| = 1.93$ for the photometer,

and $|H_{\text{LPF-S}}(0)| = 2.86$ for the spectrometer.

The overall gain of the LIA chain, relating LPF DC output voltage to the RMS JFET output voltage is given by

$$G_{\mathrm{LIA}}(w_b) = \frac{V_{\mathrm{LPF}}}{V_{\mathrm{JFET-RMS}}} = \sqrt{2}\, H_{\mathrm{Demod}}(?\, f)\left|H_{\mathrm{BPF}}(w_b)\right|\left|H_{\mathrm{LPF}}(0)\right| \quad . \tag{15}$$

For perfect phasing of the demodulator, $(\Delta f = 0)$ we have

$$G_{\mathrm{LIA}}(w_b) = (0.9003)\left|H_{\mathrm{BPF}}(w_b)\right|\left|H_{\mathrm{LPF}}(0)\right| . \tag{16}$$

This overall gain is plotted against bias modulation frequency in Figure 6.

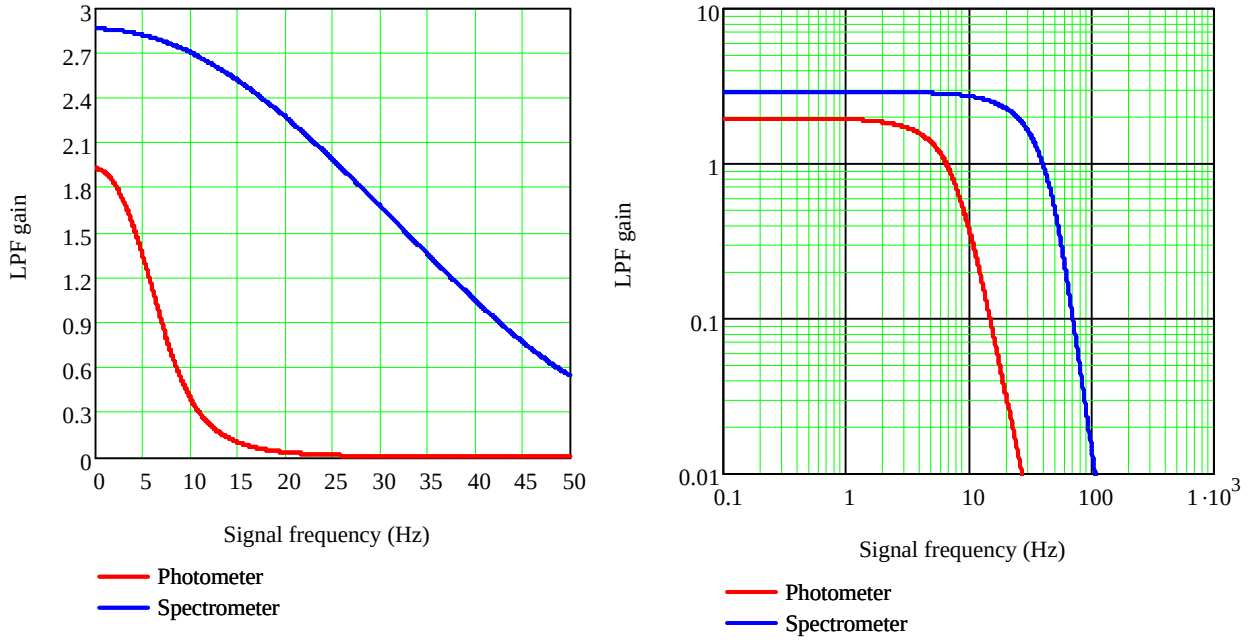

Figure 5: Low-pass filter gains as a function of detector signal frequency

For example, taking our nominal bias frequencies of 130 Hz (photometer) and 190 Hz (spectrometer), we have:

Photometer: G_{LIA} = (259.61)(1.93)(0.9003) = 451.1 (see *DCU DD* p. 44);
Spectrometer: G_{LIA} = (113.81)(2.86)(0.9003) = 293.0 (see *DCU DD* p. 57).

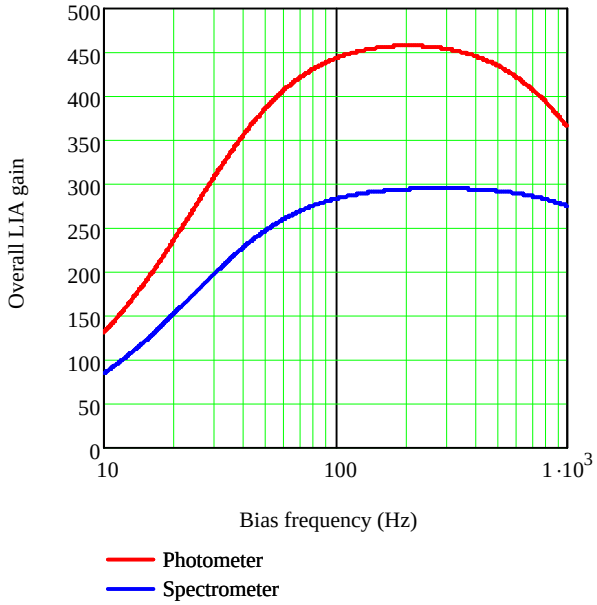

Figure 6: Overall gain of LIA signal chain, relating LPF DC output to the RMS voltage at the JFET output.

3.8 System transient response

The overall response of the system in chopped photometry mode depends on the waveform of the astronomical signal and the transient response characteristics of the detector and the low-pass filter. The astronomical signal timeline is not a pure step because of the BSM settling time and the bolometer time constant (typically 6 ms). The BSM movement between the two chop positions is quite fast, typically achieving a about 10 ms to get within 2". For simplicity, we assume a point source observation with a chop throw of 163", and a linear relationship between position and time along the trajectory, corresponding to a BSM slew rate of 1.63×10^4 "/s. For a Gaussian beam of FWHM 24" (PMW), the corresponding timeline of astronomical power on the detector is as shown in Figure 7. The signal only begins to increase towards the end of the movement as the beam moves onto the source.

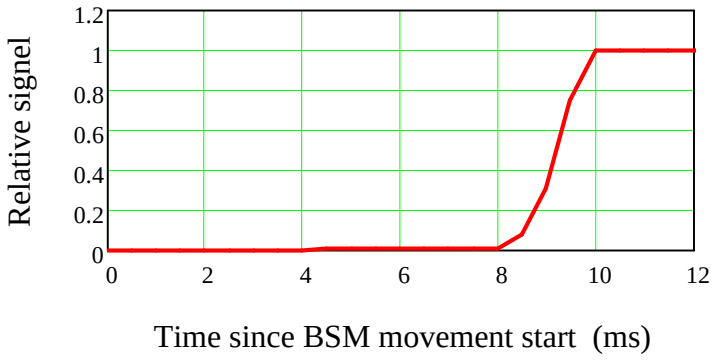

Figure 7: Simplified astronomical signal timeline for a PMW detector for a BSM movement starting at t = 0

The normalised response of the overall system to this input is shown in Figure 8. The detector time constant has been taken into account, but it is the low-pass filter that dominates the shape of the transient, and causes the significant phase delay between the BSM movement and the signal waveform.

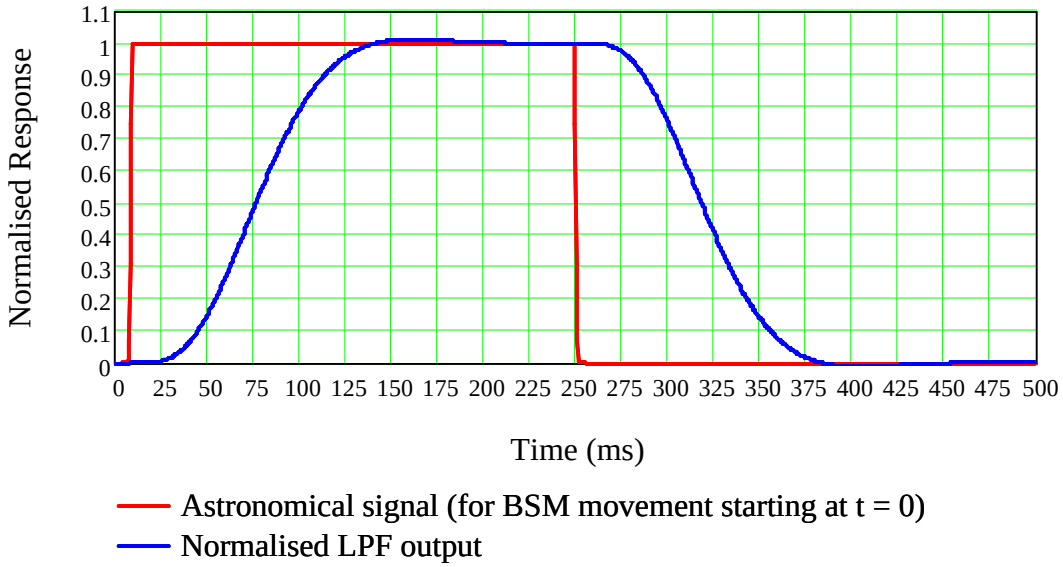

Figure 8: Overall transient response for BSM movements at t = 0 and t = 250 ms (corresponding to 2-Hz chop frequency)

The phase delay associated with the system response also introduces a delay in the signal in scan-map mode. The delay is equal to 69 ms for a Gaussian input, corresponding to a point source, with negligible distortion of the Gaussian profile. For the nominal (30 arcseconds s^{-1}) and fast (60 arcseconds s^{-1}) scan rates, this corresponds to shifts in position of 2.1" and 4.2" respectively, which must be taken into account in the map-making process.

3.9 Detector sampling and demodulation in chopped photometry mode

For detector sampling in chopped photometry mode, the sequence of events is as follows:

1. At a given time t = 0, the BSM is commanded to move (no BSM sampling or detector sampling is occurring).
2. The BSM move command is immediately followed by a command to start the BSM sampling (the delay to the first sample is always fixed).
3. After a fixed delay of t_{wait} to allow the BSM to settle down at its new position, a series of n_{samp} detector samples at frequency f_{samp} is commanded.

Note:
(i) The samples are automatically synchronised by the DCU electronics to the bias frequency $f_{b:}$ the sampling frequency is always equal to the bias frequency divided by a whole number.
(ii) There are short delays (on the order of microseconds) associated with commanding and sampling – these are ignored here.
(iii) The nominal value of n_{samp} is 4 (i.e., 8 samples in total per BSM cycle) to ensure adequate sampling of the waveform and to keep within the allowed data rate. With 2-Hz chop frequency and 4 samples per half-cycle, the samples are not statistically independent – there is little penalty in principle if they are not all used in the demodulation.
(iv) The actual time of the first sample will be greater than the time of the command due to the synchronism with the bias waveform. We assume that there will be a pseudo-random delay of up to one bias period, T_b, (typically 8 ms for a bias frequency of 130 Hz).
(v) The final sample in the set of n_{samp} need not be taken before the BSM is commanded to move again.

The chopped signal demodulation scheme must divide the signal waveform into two equal intervals phased in such a way as to maximise the demodulated signal level (i.e., it needs to be phase-synchronous).

Taking these considerations into account, the recommended sampling scheme for a particular case is described below.

Bias frequency:	f_b = 130 Hz								
Bias period:	$T_b = 1/f_b$ = 7.68 ms								
Number of samples per BSM position:	n_{samp} = 4								
Sampling frequency:	$f_{samp} = f_b/7$ = 18.60 Hz								
Time between samples	$T_{samp} = 1/f_{samp}$ = 53.76 ms								
Delay between BSM movement command and sample 1	t_{wait} = 95 ms								
Commanded times of the eight samples	95.0	148.8	202.5	256.3	345.0	398.8	452.5	506.3	ms
Latest possible times of the samples	102.7	156.4	211.0	264.0	352.7	406.4	460.2	514.0	ms

The waveform and sample times are shown in Figure 9. The black and pink dots are separated by the bias period, T_b, and represent the extremes that may occur. Note that the possible delay in the range $(0 – T_b)$ could be different for the positive and negative half cycles.

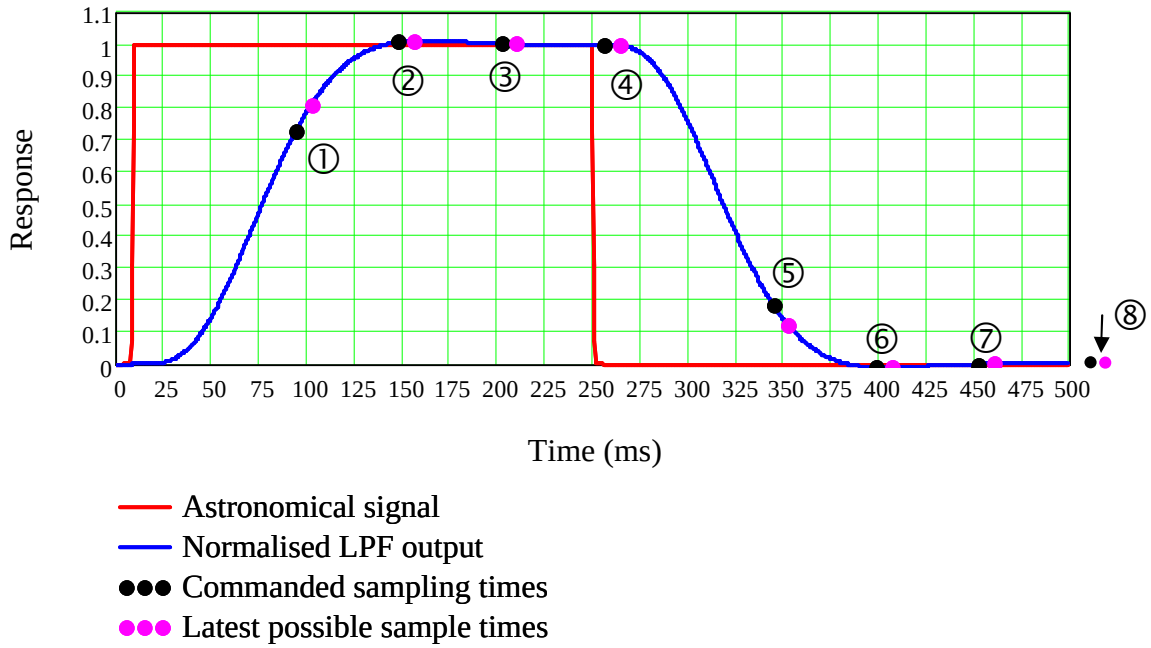

Figure 9: Eight signal samples over one BSM cycle for the example given in the text.

Because of the unpredictability of exactly when the samples are going to occur, the samples taken during the rise or fall period can vary significantly, making it inappropriate to use these for signal demodulation. Here we assume that the last three samples for each BSM position are to be used - i.e., samples sets (2, 3, 4) and (6, 7, 8) above. The demodulated signal is then simply computed as the sum of samples 2, 3 and 4 minus the sum of samples 6, 7 and 8. In order to make the results insensitive to the potential variation in sampling times, it is necessary to optimise the delay between BSM motion and the initiation of the sampling sequence such that the three samples lie securely on the flat part of the waveform. Calculations have been done to determine the optimum value of t_{wait} and the corresponding variation in derived signal level arising from all possible

combinations of delays in each half cycle. The demodulated signal varies by less than 0.1% over the whole range of possible sample distributions.

Note:

(i) although the first sample in each half cycle is not used explicitly in the demodulation, it can be used for monitoring/diagnostic purposes if appropriate;

(ii) the detailed sample timings will depend on the precise bias frequency and chop frequency adopted - the example above illustrates the method for devising the sampling and demodulation schemes;

(iii) it would be desirable to have five samples per half-cycle if the telemetry rate permits.

3.10 Multiplexer

The LIA outputs are multiplexed in groups of 16 (photometer) or 12 (spectrometer). In the case of the photometer, a second stage of multiplexing combines three groups of 16 to form a group of 48 channels.

3.11 Offset subtraction

After multiplexing, a pre-determined offset is subtracted for each channel. Offset subtraction is needed because the signals need to be sampled with greater precision than the 16 bits available from the ADC. This is achieved by subtracting a suitable DC offset from each signal and adding in an additional gain stage before digitisation. The offset voltage is generated by the DCU from a 4-bit DAC with binary input value *OFFSET* (range = 0 – 15).

At the start of each observation, the value of *OFFSET* is set for each detector individually by the DCU according to a procedure described in Section 3.12 below. It is not possible to change the offsets during an observation, so the settings must be able to cope with the entire range of detector power expected during the observation – this includes changes due to the astronomical signal (all observing modes) and due to signal offsets created by chopping (point source and jiggle-map modes).

After offset subtraction, the signal is amplified by a gain of 12 and then digitised, producing a binary output value *DATA*, with range 0 to $(2^{16} - 1)$, which is sent to the DPU for telemetry.

The total gain of the DCU chain is thus $G_{\rm tot}(w_{\rm b}) = 12G_{\rm LIA}(w_{\rm b})$. For the nominal bias frequencies used above, we therefore have

Photometer:	$G_{\rm tot}$ = (12)(451.1)	=	5413	(see *DCU DD* p. 77);
Spectrometer:	$G_{\rm tot}$ = (12)(293.0)	=	3517	(see *DCU DD* p. 77).

For bias frequency $w_{\rm b}$, the RMS voltage at the BPF input (i.e., the JFET output) is related to the digital ADC output, *DATA*, and the offset level, *OFFSET*, by the following formula (*DCU DD* p. 77):

$$V_{\rm JFET-RMS}(w_{\rm b}, DATA, OFFSET) = \left[\frac{5}{G_{\rm tot}(w_{\rm b})}\right]\left[\frac{Data - 2^{14} + (52428.8)(OFFSET)}{(2^{16}-1)}\right]. \qquad (17)$$

This voltage is in turn related to the RMS bolometer voltage by

$$V_{\rm JFET\text{-}RMS}(w_{\rm b}) = H_{\rm H}(w_{\rm b}) H_{\rm JFET}\, V_{\rm d\text{-}RMS}\,. \qquad (18)$$

To see how the RMS voltage at the JFET output is related to the ADC output and offset setting, $V_{\text{JFET-RMS}}$ is plotted in Figure 10 for the case of the nominal photometer gain, G_{tot} = 5413 (note that the numbers given in the *DCU DD p. 77* correspond to the maximum gain of 5481). For this gain value, each offset step corresponds to a range of 0.924 mV and the 15 available offset levels cover a range up to 11.71 mV, with some overlap between successive offset levels, as indicated in Table 1.

There are 2^{16} - 1 = 65535 ADC bits potentially available within each *OFFSET* range, so the voltage step corresponding to one bit is

$$\Delta V_{\text{JFET-RMS}}(1 \text{ bit}) = (0.924 \text{ mV})/(65535) = 14.07 \text{ nV} . \qquad (19)$$

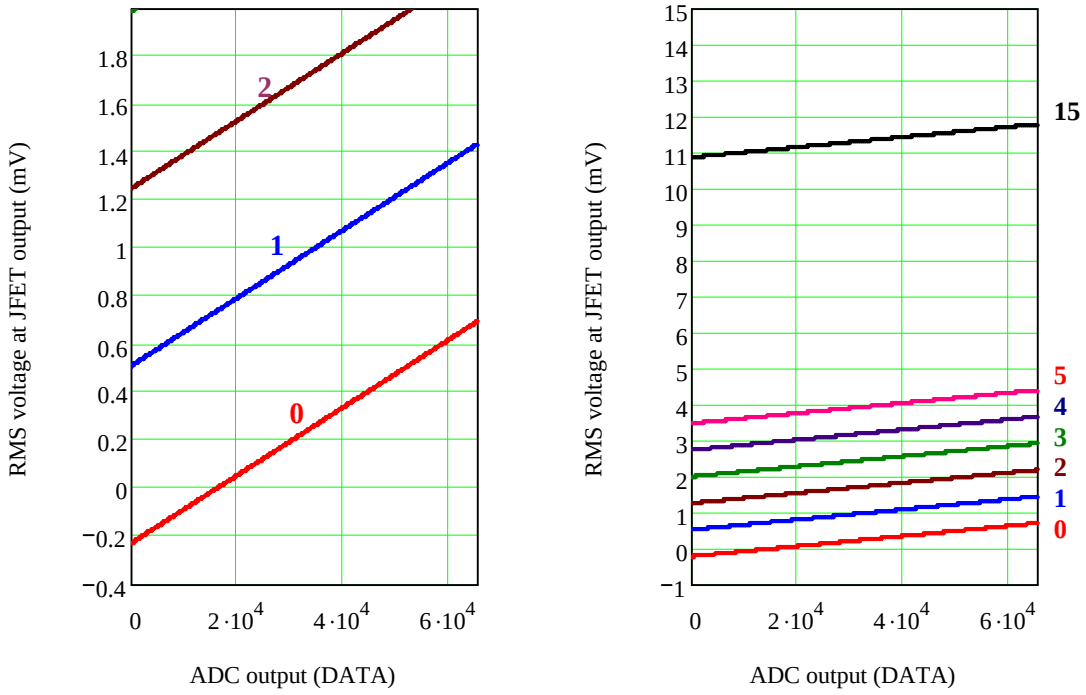

Figure 10: Photometer ADC output vs. JFET RMS output voltage for various values of OFFSET (for G_{tot} = 5413)

Offset =	Lower limit (mV) $V_{JFETrms}(0, Offset, G)$ =	Upper limit (mV) $V_{JFETrms}(2^{16} - 1, Offset, G)$
0	-0.2309	0.6927
1	0.5080	1.4317
2	1.2469	2.1706
3	1.9859	2.9095
4	2.7248	3.6485
5	3.4637	4.3874
6	4.2027	5.1263
7	4.9416	5.8652
8	5.6805	6.6042
9	6.4195	7.3431
10	7.1584	8.0820
11	7.8973	8.8210
12	8.6362	9.5599
13	9.3752	10.2988
14	10.1141	11.0378
15	10.8530	11.7767

Table 1: $V_{JFET\text{-}RMS}$ range covered by each OFFSET value for the photometer with G_{tot} = 5413.

3.12 Offset setting procedure

Before each observation, the offsets are set for all detectors according to the procedure shown in Figure 11 (see *DCU DD* p. 126). The procedure is designed to ensure that the most significant bit of *DATA* is zero.

For a given value of $V_{JFET\text{-}RMS}$ at the start of the observation:

1. *DATA* is a 16-bit number with range 0 to $2^{16} - 1$, with the bits numbered 0 – 15.
2. The 4-bit *OFFSET* is first set to 0000.
3. *OFFSET* is then incremented until bit-15 of *DATA* = 0 (i.e., until *DATA* is less than 2^{15})
4. Provided bits 13-15 of *DATA* are not all zero, this value of *OFFSET* is selected.
5. If bits 13-15 of *DATA* are all zero (i.e., if *DATA* < 10^{13}) and OFFSET ≠ 0, then *OFFSET* is decreased by one and then selected. This ensures a worst-case dynamic range of 13 bits (8192).

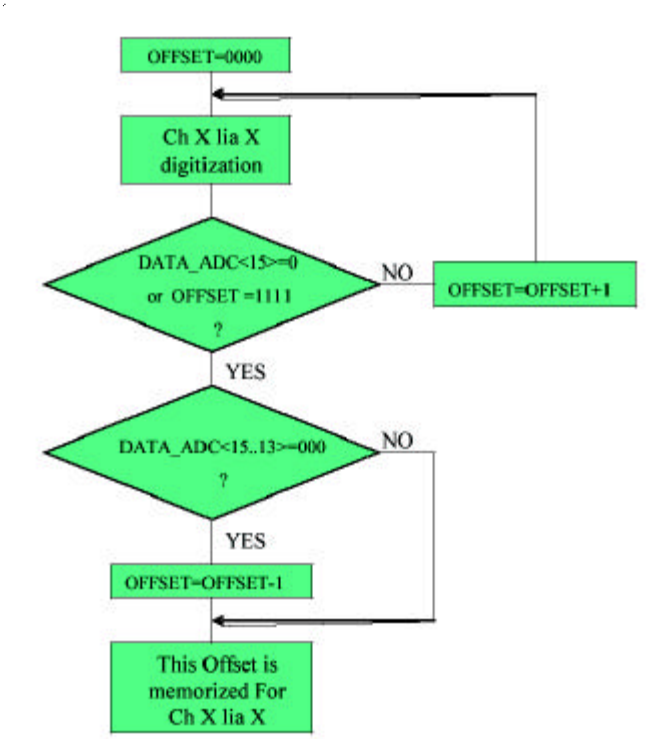

Figure 11: Procedure for setting the value of O*FFSET*

This procedure is completely deterministic in that a given value of $V_{\text{JFET-RMS}}$ will result in a particular value of *OFFSET* being selected. Table 2 lists the selected *OFFSET* values as a function of $V_{\text{JFET-RMS}}$ for the case of the photometer with G_{tot} = 5481, and the chosen *OFFSET* is plotted against $V_{\text{JFET-RMS}}$ in Figure 13. The actual voltage range per level (i.e., upper – lower voltage for a given selected offset is 0.7298 V).

Note that when $V_{\text{JFET-RMS}}$ is just above an offset threshold, the value of *DATA* is 8192, and when it is just below an offset threshold, *DATA* is at its maximum allowed value (before changing the offset) of 60620, as shown in Figure 12.

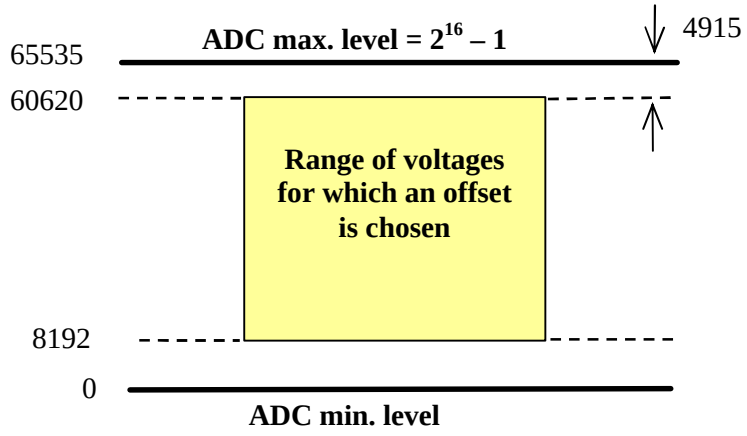

Figure 12: Range of ADC output values corresponding to one offset setting.

If the voltage increases during the observation, then in the worst case, the available dynamic range is 4915 bits, and if the voltage decreases during the observation, the worst case dynamic range is 8192 bits.

To illustrate this, consider first the case of $V_{\text{JFET-RMS}}$ = 1.36239 mV (Table 2):

- This is just large enough to make *OFFSET* = 2, and the corresponding value of *DATA* = 8192
- For *OFFSET* = 2, the ADC zero level corresponds to $V_{\text{JFET-RMS}}$ = 1.2469 mV (Table 1).
- The corresponding dynamic range is 1.36239 - 1.2469 = 0.115 mV.
- The same “worst case” dynamic range applies to all offset settings.

Now consider the case of $V_{\text{JFET-RMS}}$ = 1.36238 mV (Table 2)

- This is the highest value that will make *OFFSET* = 1, and the corresponding value of *DATA* = 60620.
- For *OFFSET* = 1, the ADC zero level corresponds to $V_{\text{JFET-RMS}}$ = 0.5080 mV (Table 1).
- The corresponding dynamic range is 1.36238 – 0.5080 = 0.854 mV.
- The same “best case” dynamic range applies to all offset settings.

Offset o =	Voltage range (mV) for which this offset is chosen: vL_o =	vU_o =	ADC zero level for this offset: $V_{JFETrms}(0, Offset, G)$ =	ADC max. level for this offset: $V_{JFETrms}(2^{16}-1, Offset, G)$ =	G = 5413: $DATA(vL_j, j, G)$ =	$DATA(vU_j, j, G)$ =
0	-0.11547	0.62347	-0.230916	0.693	8191	60621
1	0.62346	1.36240	0.508014	1.432	8191	60621
2	1.36239	2.10133	1.246944	2.171	8191	60621
3	2.10132	2.84026	1.985874	2.910	8191	60621
4	2.84025	3.57919	2.724804	3.648	8191	60621
5	3.57918	4.31812	3.463734	4.387	8191	60621
6	4.31811	5.05705	4.202663	5.126	8191	60621
7	5.05704	5.79598	4.941593	5.865	8191	60621
8	5.79597	6.53491	5.680523	6.604	8191	60621
9	6.53490	7.27384	6.419453	7.343	8191	60621
10	7.27383	8.01277	7.158383	8.082	8191	60621
11	8.01276	8.75170	7.897313	8.821	8191	60621
12	8.75169	9.49063	8.636242	9.560	8191	60621
13	9.49062	10.22956	9.375172	10.299	8191	60621
14	10.22955	10.96849	10.114102	11.038	8191	60621
15	10.96848	11.70742	10.853032	11.777	8191	60621

Table 2: Offset values and the ranges of $V_{JFET\text{-}RMS}$ for which they will be selected (photometer with G_{tot} = 5413)

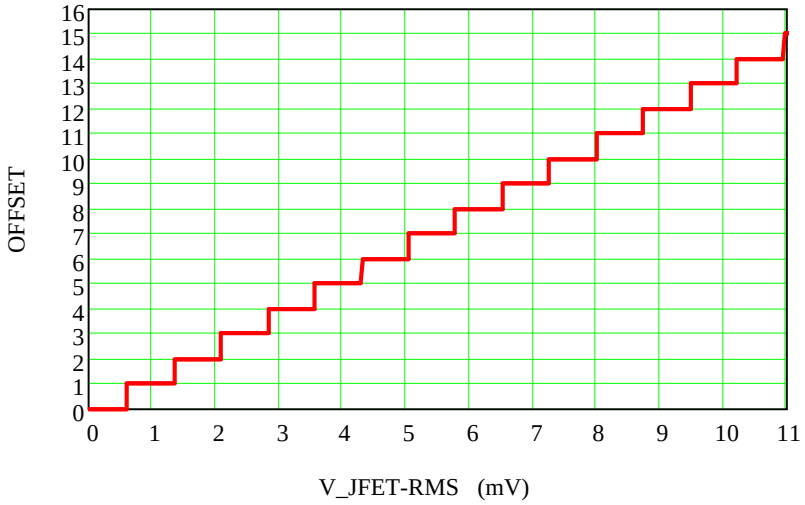

Figure 13: Selected OFFSET vs. $V_{JFET\text{-}RMS}$ (photometer with G_{tot} = 5413)

3.13 Offset setting for the photometer

Consider an observation during which the source flux density will vary between $S_{v\text{-}min}$ and $S_{v\text{-}max}$. Before the observation, the *OFFSET* value will be set up for each detector, determined by its output voltage. Offsets can be set either off-source (default for the photometer) or on-source.

Off-source case: the nominal situation is that $S_v = S_{v\text{-}min} = 0$, so that $V_{JFET\text{-}RMS} = V_o$ at the telescope position for which the offsets are set. While the observations are in progress, the bolometer output voltage is always less than the value when the offset is selected - $V_{JFET\text{-}RMS}$ moves towards the zero level of the ADC, with a maximum change ΔV, as shown in Figure 14.

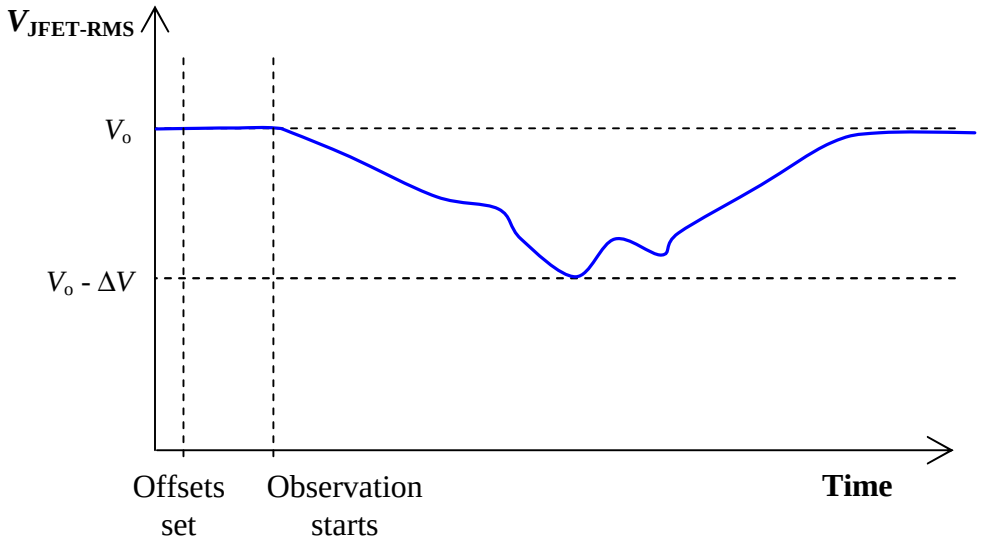

Figure 14: Example signal voltage timeline with offsets set at zero signal before the observation.

The worst case dynamic range corresponds to the case in which the V_o is just above an offset threshold, so that *DATA* = 8192 and the difference between it and the value that will give *DATA* = 0 is at its smallest: the allowed drop in detector voltage during the observation is therefore at its smallest.

The worst case dynamic range is $8192 \times \Delta V_{JFET-RMS}(1 \text{ bit}) = (8192)(14.09 \text{ nV}) = 0.115 \text{ mV}$.

The best case dynamic range corresponds to the case in which the $V_{JFET-RMS}$ is just below an offset threshold, so that *DATA* = 56525 and the difference between it and the value that will give *DATA* = 0 is at its largest: the allowed drop in detector voltage during the observation is therefore at its largest.

The best case dynamic range is $60620 \times \Delta V_{JFET-RMS}(1 \text{ bit}) = (60620)(14.09 \text{ nV}) = 0.854 \text{ mV}$.

To get a rough estimate of the corresponding source brightness limits, the SPIRE photometer sensitivity model (assuming 20 mV rms bias voltage for all arrays) has been used to derive the following information:

Band	Total background power (mainly from the telescope) (pW)	Astronomical gain (Jy pW^{-1})	Responsivity (MV W^{-1})	Worst case dyn. range of 0.115 mV expressed in pW	Worst case dynamic range in Jy
PSW	1.2	137	320	0.36	(0.36)*137 = 49
PMW	1.0	250	330	0.35	(0.35)*250 = 87
PLW	1.7	226	350	0.33	(0.33)*226 = 74

So the worst case dynamic range corresponds to between about 50 and 100 Jy. The best case limits are about six times larger, so objects brighter than several hundred Jy will pose problems with saturation unless the detector bias is adjusted.

General case: Let the offsets be set at a position for which the flux density is some fraction *h* of the total range – i.e., $S_v = h(S_{v\text{-max}} - S_{v\text{-min}})$. The value of *h* can be different for each detector as they view different parts of the sky. $V_{JFET-RMS}$ can now increase of decrease during the observations.

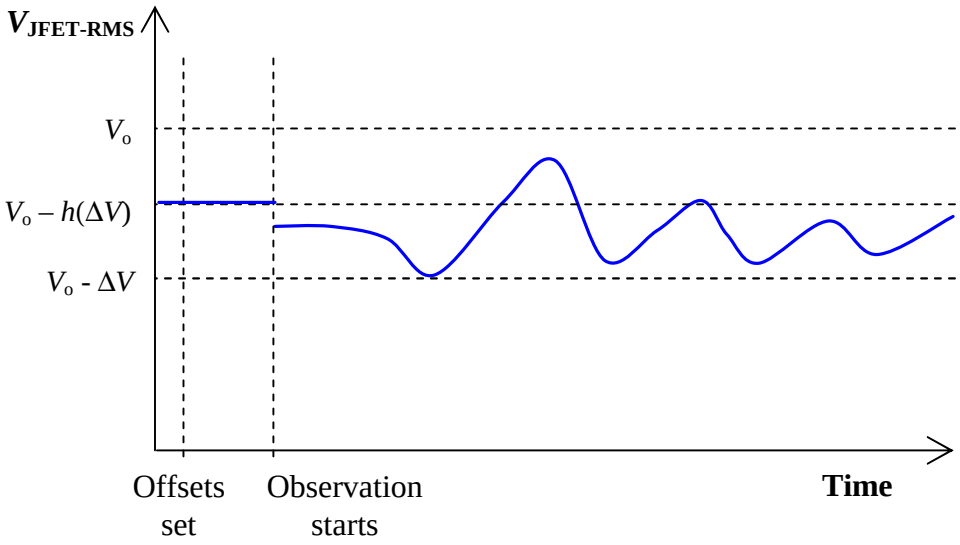

Figure 15: Example signal voltage timeline with offsets set at an intermediate signal level before the observation

In this case, the offsets are set at $V_{JFET\text{-}RMS} = V_o - h(\Delta V)$. The dynamic range requirement for increasing sky signal (decreasing output voltage) is now less than before, which is good. However, during parts of the observation, the voltage will also be higher than the initial value, by an amount up to $h(\Delta V)$. In the worst case, the available dynamic range for this is only 4915 bits.

Since in the general case it will not be convenient or feasible to set the offsets at some intermediate brightness level, the default option will be to set them off-source, which should in most cases correspond to the a sky brightness less than or equal to the faintest part of the observation (so that for all detectors, $V_{JFET\text{-}RMS}$ only decreases during the observation).

3.14 Offset setting for the FTS

Assume for simplicity that the telescope is perfectly nulled by SCal (in practice there will be a small imbalance). Under that condition, an observation of blank sky results in a null interferogram – the power absorbed by the detector is constant throughout the interferogram at $(1/2)(Q_{Tel} + Q_{SCal})$. = Q_{Tel}, and the corresponding output voltage is constant at V_o. Now let a source be observed which results in an increase ΔQ in the broadband continuum power coming through the telescope. This will be split equally between the output ports, increasing the continuum power absorbed by the detectors. The unmodulated output voltage (corresponding to the DC level in the wings of the interferogram) will thus decrease by some corresponding – let this be $\Delta V/2$ (corresponding to $\Delta Q/2$).

When the mirror is scanned, the resulting interferogram represents the difference between the telescope and SCal input ports. One output port will correspond to (Telescope + Sky) – SCal, and the other to SCal – (Telescope + Sky). In the former case, the interferogram will have a negative-going central maximum (more radiant power), and in the latter case a positive-going central maximum (less radiant power). The peak height of the interferogram is equivalent to the continuum level, and so is also $\Delta V/2$. The two possible interferograms are illustrated in Figure 16. The total dynamic range that must be available to be able to cope with either case is V_o to $V_o - \Delta V$.

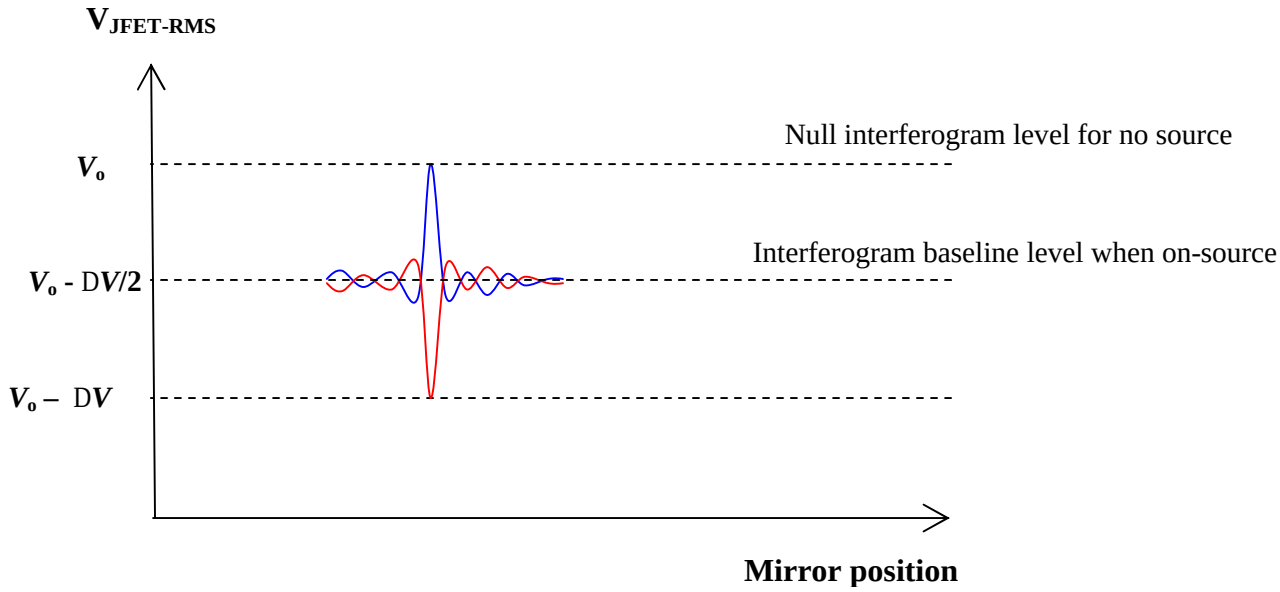

Figure 16: Interferogram dynamic range, assuming perfect nulling of the telescope. The output voltage is V_o for no source, and (V_o – $\Delta V/2$) off ZPD when on source. The red interferogram is for the port corresponding to (Telescope + Sky) – SCal, and the blue on is for the port corresponding to SCal – (Telescope + Sky).

Offsets set of-source (i.e., at V_o): The output voltage will always decrease. When the telescope is pointed on-source, the interferogram baseline level will be V_o – $\Delta V/2$, and we must be able to cope with a change of $\pm \Delta V/2$ about that level. In the worst case, with the offset set initially at the bottom of its range, the highest continuum level that can be coped with corresponds to (8192)/2 = 4096 bits.

Offsets set on-source (i.e., at V_o – DV/2): The output voltage can now go up or down in the interferogram. If the offset is set at the bottom of the range, the output can go down by 8192 bits. If it's set at the top, the output can go up by 4195 bits.

So setting the offsets on-source has a slight advantage in terms of the worst-case dynamic range.

3.15 Measurement of detector voltage, current, and resistance

From equation (17), the RMS voltage at the JFET output can be computed from the telemetry data value. This can be used to derive the detector voltage, current and resistance by an iterative procedure designed to take into account the *RC* roll-off due to the harness transfer function (equations 5 and 6) and also any changes in the phasing of the demodulator.

Step 1: Estimate $I_{b\text{-}RMS}$ and R_d, taking $H_H(w_b) = 1$:

$$I_{b-RMS} = \frac{V_{b-RMS} - \left(\frac{V_{JFET-RMS}}{H_{JFET}}\right)}{R_L} \quad \text{and} \quad R_d = \frac{V_{b-RMS}}{I_{b-RMS}} - R_L . \qquad (20)$$

Step 2: Estimate $H_H(w_b)$ and Δf:

$$\left|H_{\rm H}(w_{\rm b})\right| \;=\; \frac{1}{\left[1+(w_{\rm b}t_{\rm H})^2\right]^{1/2}} \qquad \text{and} \quad ?f \;=\; \tan^{-1}(w_{\rm b}t_{\rm H})\,, \tag{21}$$

$$\text{with} \quad t_{\rm H} = \left[\frac{R_{\rm L}R_{\rm d}}{R_{\rm L}+R_{\rm d}}\right]C_{\rm H}\,.$$

Step 3: Recalculate $I_{\rm b\text{-}RMS}$ and $R_{\rm d}$:

$$I_{\rm b-rms} \;=\; \frac{V_{\rm b-rms} - \left(\dfrac{V_{\rm JFET-RMS}}{H_{\rm JFET}\left|H_{\rm H}(w_{\rm b})\right|\cos(?f)}\right)}{R_{\rm L}} \qquad \text{and} \qquad R_{\rm d} \;=\; \frac{V_{\rm b-RMS}}{I_{\rm b-RMS}} - R_{\rm L}\,. \tag{22}$$

Continue iterating (repeat steps 2 and 3) until $I_{\rm b\text{-}RMS}$ and $R_{\rm d}$ converge (criterion: change on iteration < 0.1%).

The RMS detector voltage is then just $$V_{\rm d\text{-}RMS} \;=\; I_{\rm b-RMS}\,R_{\rm d}\,. \tag{23}$$

The timelines of voltage and current constitute the Photometer Data Timeline (PDT) products.

4. Photometer signal pipeline

In this section we outline two proposed implementations of the photometer signal pipeline for conversion of detector signals to in-beam source flux density.

Model-based pipeline: this works in terms of the radiant power absorbed by the detectors, automatically takes into account the detector bias conditions, non-linear response to strong sources, and any variations in detector bath temperature and background radiation from the instrument or the telescope.

Empirical pipeline: this is similar to the data processing schemes traditionally used for bolometer instruments, and works in terms of detector voltage rather than radiant power. Corrections are needed in the case of non-linear response to high signal levels, and are implemented by suitable bias-specific calibration files based on bolometer modelling and/or astronomical measurements. The removal of thermal variations is effected using correlations between the detector signals themselves and/or thermometry data.

These two approaches are described in detail in Sections 4.1 and 4.2 below. It is proposed that the pipeline architecture be consistent with both options. Implementing the model-based pipeline may be challenging, at least in the first instance, so it is proposed that the simple version be implemented in full and available at the start of the mission.

4.1 Model-based photometer pipeline

4.1.1 First-level deglitching

Before further processing of the measured detector voltage timeline, glitches due to cosmic ray hits or other impulse-like events in the detectors will be removed.

Two options are considered:

Option 1: A simple algorithm is implemented in which the signature of the system response to an impulse (above some specified threshold which will depend on the noise level) is registered. The corresponding data samples are removed from the timeline and/or flagged as corresponding to a glitch.

Option 2: A more sophisticated approach is described in Ref. [2] and proposed for the FTS, based on a local regularity analysis combined with a wavelet analysis. This scheme needs to be evaluated for use in the photometer pipeline. In principle, the same method should be applicable in both pipelines.

For the moment, we assume that Option 2 is to be implemented for the photometer also.

4.1.2 Determination of the total radiant power absorbed by a detector

The SPIRE detectors can be accurately modelled as ideal thermal bolometers, based on the model of Mather [3] as codified by Sudiwala *et al*. [4]. The bolometer parameters (T_g, T_o, R_S, $G_{d\text{-}300mK}$, and b) are known for each detector individually. Measurements of the bolometer electrical parameters can be used to determine the first estimate of the absolute absorbed radiant power, Q_1, as follows.

$$P = V_{d\text{-}RMS} I_{b\text{-}RMS} \ , \tag{24}$$

$$R_d = \frac{V_{d\text{-}RMS}}{I_{b\text{-}RMS}} \ , \tag{25}$$

$$T = \frac{T_g}{\left[ln\left(\frac{R_d}{R_S} \right) \right]^2} , \tag{26}$$

The dynamic thermal conductance follows a power law variation with temperature (Sudiwala *et al*., eqt. 12):

$$G_d(T) \propto T^b \tag{27}$$

For the SPIRE bolometers, the thermal conductance is specified at a nominal temperature of 300 mK, so

$$G_d(T) = G_{d-300mK}\left[\frac{T}{0.3} \right]^b . \tag{28}$$

The total power dissipated in the bolometer is

$$W = P + Q = \int_{T_o}^{T} G_d(T) dT = \frac{G_{d-300mK}}{(0.3)^b} \int_{T_o}^{T} T^b \, dT . \tag{29}$$

So

$$Q_1 = \frac{G_{d-300mK}}{(0.3)^b (b+1)} \left(T^{b+1} - T_o^{\,b+1} \right) - P . \tag{30}$$

If the bolometer is in the linear (small signal) regime, then a change in Q, ΔQ, is linearly proportional to the corresponding change in bolometer voltage ΔV, through the responsivity ($\Delta V/\Delta Q$).

4.1.3 Removal of correlated noise due to temperature fluctuations (scan-map only)

To first order, bath temperature fluctuations will influence all detectors in an array coherently – the temperature and corresponding output voltages will go up and down in synchronism. The bath temperature, T_o, may fluctuate due to temperature drifts within the instrument, and a timeline for T_o must be generated in order to implement equation (29). For the level of fluctuations expected in SPIRE, the most important effect of bath temperature variations will be the direct response of the detector output voltage. There will be a small second-order effects on the detector small-signal responsivity. In the case of the model-based pipeline, this is automatically corrected in any case.

Fluctuations in T_o are expected to be much slower than the nominal chopping frequency of 2 Hz, so that the correction will only be needed for scan-map observations.

The following approach is proposed for scan-map data:

A single bath temperature timeline, $T_o(t)$, is generated for each array – we assume that there are no differences in bath temperature within an array. The timelines are produced by a TBD algorithm from thermometric information (based on some or all of two blind detectors and thermometers on each array, and the ^{3}He fridge thermometry).

An important issue for the $T_o(t)$ algorithm is that in order not to introduce additional noise, the temperature timeline will need to be significantly less noisy than the bolometer signals. It will therefore need to be averaged over a period of time such that it becomes a negligible fraction (say 10%) of the detector noise – this may requires an averaging periods several tens of seconds. Thermal fluctuations on timescales shorter than this will not be tracked.

4.1.4 Removal of electrical crosstalk

Let the value of absorbed power for detector i (after subtraction of correlated temperature fluctuations) be $Q_{1\text{-}i}$. $Q_{1\text{-}i}$ might contain contributions that depend on the signals from other detectors due to either electrical or optical crosstalk. Electrical crosstalk arises after the detector and is due to capacitative or inductive coupling between the detector readout channels. Optical crosstalk occurs before the detector and is due to diffraction or aberrations in the optical system causing some of the power from an astronomical source to fall on inappropriate detectors.

Electrical crosstalk can be removed if the coupling between the detectors is known, and it is appropriate to do it at this stage. The removal of optical crosstalk can only be done after the constant telescope background has been subtracted (see Section 4.1.6).

Here we assume that

(i) electrical crosstalk is linear, so that the effects can be characterised by a crossstalk matrix, $\mathbf{C_{elec}}$, with constant elements;
(ii) electrical crosstalk from one detector to another does not result in any diminution of the signal in the primary detector;
(iii) there is no crosstalk between different arrays.

The vector of electrical crosstalk-corrected signals is given by

$$\mathbf{Q}_2 = \mathbf{C_{elec}}\,\mathbf{Q}_1 . \qquad (31)$$

As an illustration, if we had thee detectors, the matrix equation would be

$$\begin{bmatrix} Q_{2-1} \\ Q_{2-2} \\ Q_{2-3} \end{bmatrix} = \begin{bmatrix} 1 & e_{21} & e_{31} \\ e_{12} & 1 & e_{32} \\ e_{13} & e_{23} & 1 \end{bmatrix} \begin{bmatrix} Q_{1-1} \\ Q_{1-2} \\ Q_{1-3} \end{bmatrix}. \quad (32)$$

The electrical crosstalk matrix can be implemented as a calibration file. Determination of the elements of the electrical crosstalk matrix is a difficult problem. One possibility is to use the occasional ionising radiation hits that the bolometers will experience. Ideally, a single event in a bolometer produces a spike only in its own output; crosstalk results in this being accompanied by lower-level responses from other detectors.

In the absence of crosstalk, or if the crosstalk correction is to be left out, then the e_{ij} coefficients are set to zero.

4.1.5 Subtraction of background power

The absorbed power will have two contributions, one from the source, Q_S , and one from the telescope and instrument background, Q_B , with

$$Q = Q_S + Q_B . \quad (33)$$

Q_B must therefore be subtracted. It can have contributions from the telescope and the instrument (particularly the Level-1 box).

Point source and jiggle map observations: In the case of chopped photometric observations, background subtraction is done naturally in the course of the demodulation of the nodded timelines, as illustrated in Figure 17 (adapted from the SPIRE OMD).

Absorbed power from the source	$= Q_S$
Absorbed power from the background in chop position R	$= Q_{BR}$
Absorbed power from the background in chop position L	$= Q_{BL}$
De-modulated chopped signal for nod position A	$= (Q_S + Q_{BR}) - Q_{BL}$
De-modulated chopped signal for nod position B	$= Q_{BR} - (Q_S + Q_{BL})$
Difference (de-modulated nod signal)	$= (Q_S + Q_{BR}) - Q_{BL} - Q_{BR} + (Q_S + Q_{BL}) = 2Q_S$

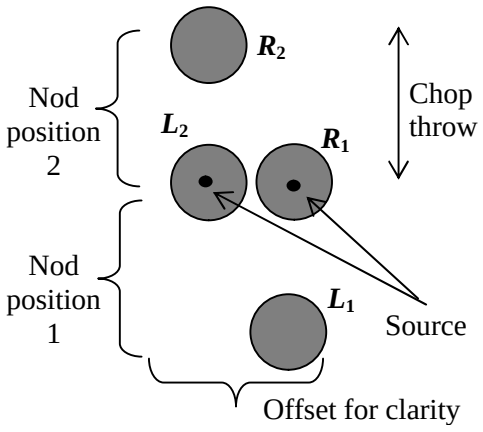

Figure 17: Nodding and corresponding removal of signal offsets

The nominal method to be used to demodulate the chopped signal is described in Section 3.9. In the case of chopped observations, second-level deglitching can also be carried out after demodulation, by median filtering of the demodulated samples corresponding to the same sky position.

Scan-map observations: The most challenging case for background subtraction is that of large area maps from which it is desired to extract extended sky structure. The following approach is proposed.

Standard calibration observations are carried out of "dark" areas of sky using scan-map mode, to produce a calibration file corresponding to the absorbed background levels for the detectors under the nominal conditions ("dark sky", known telescope and Level-1 temperatures).

A TBD algorithm is then implemented, which uses these calibration files and makes any small corrections for different telescope and L-1 temperatures during the source observation (compared to the calibration observation) to calculate Q_B for each detector for the particular conditions applying to the source observation.

The first estimate of the signal power timelines $Q_{S1}(t)$ can then be calculated by subtracting this from the measured timeline $Q_2(t)$.

Removal of the telescope background in this way involves subtracting a fixed offset for each detector. In most instances, this offset will be much larger than the astronomical power levels, so that great precision would be needed in order to correct in an absolute manner. We assume, therefore, that residual offsets will remain in the data that must be removed later in the analysis. The most effective method is to carry out the background removal as part of the map-making process. With cross-linked maps, which are recommended for most scan-map observations, this is done naturally as part of the map-making routine. It may be most convenient to defer any attempt to remove the background to the map-making stage, but the capability of implementing a preliminary background cancellation at this stage in the pipeline.

Alternative approaches are:

(i) fit a slope and intercept to each detector scan and remove the corresponding baseline;
(ii) fit a baseline only to portions of the scan at the beginning and the end.

The first method risks removing real sky structure as it may affect the slope. The second method may be less vulnerable to that, but only if the area covered is large enough that the peripheral parts represent a plane of background emission that can be subtracted without affecting structure of genuine interest to the observer.
Neither of these methods should be implemented until the map-making stage.

4.1.6 Removal of optical crosstalk

Optical crosstalk is here defined as power that should be incident on one detector actually falling on another. It is important to note that in the case of SPIRE, neighbouring detectors are separated by an angle of $2\lambda/D$ on the sky, and even if a source is on-axis for a given pixel, some fraction of the source power will be incident on the neighbouring detectors due to telescope diffraction. Non-neighbouring detectors are sufficiently far apart that they should not pick up any power from an on-axis source.

Optical crosstalk can be characterised by a crosstalk matrix, $\mathbf{C_{opt}}$, analogous to the electrical crosstalk matrix described in Section 4.1.4.

The vector of optical crosstalk-corrected signals is given by

$$\mathbf{Q_{S2}} = \mathbf{C_{opt}}\,\mathbf{Q_{S1}}\,. \qquad (34)$$

As an illustration, if we had thee detectors, the matrix equation would be

$$\begin{bmatrix} Q_{\text{S2-1}} \\ Q_{\text{S2-2}} \\ Q_{\text{S2-3}} \end{bmatrix} = \begin{bmatrix} o_{11} & o_{21} & o_{31} \\ o_{12} & o_{22} & o_{32} \\ o_{13} & o_{23} & o_{33} \end{bmatrix} \begin{bmatrix} Q_{\text{S1-1}} \\ Q_{\text{S1-2}} \\ Q_{\text{S1–3}} \end{bmatrix}$$

Unlike the case of electrical crosstalk, the diagonal elements are not equal to unity since optical crosstalk involves loss of power from the primary detector.

The optical crosstalk matrix can be implemented as a calibration file. The values of o_{ij} must be determined from calibration observations involving scanning a strong point source across each of the detectors in the array.

In the absence of optical crosstalk, or if the crosstalk correction is to be left out, then the non-diagonal o_{ij} coefficients are set to zero and the diagonal coefficients are set to unity.

4.1.7 Correction for beam smearing due to scan speed (scan-map only)

The overall speed of response of a detector channel depends on the bolometer time response and the low-pass filter in the electronics chain. Spatial frequencies on the sky are encoded as electrical frequencies in the detector output in a manner that depends on the beam size and the telescope scan speed. For the fastest Herschel scan speed of 60" s^{-1} and the smallest SPIRE beam FWHM of 18" (for PSW), the beam crossing time is 18/60 s = 300 ms. The LPF has a 3-dB frequency of approximately 5 Hz, corresponding to a time constant of approximately 30 ms The basic detector time constant is typically 6 ms, so the filter should be the dominant effect, and with a time constant ~ ten times faster than the beam crossing time, the distortion should be negligible. However, there is now evidence from measurements on similar detectors (used on Planck-HFI, BLAST, and BICEP) that SPIRE-like bolometers can exhibit a low-level slow response. The overall detector-filter chain must be characterised by an appropriate transfer function, which will need to be measured after launch.

The baseline plan is to correct for this beam smearing effect in the pipeline, at this stage in the processing chain. The correction is implemented by Fourier transforming the detector timeline, multiplying the FT by an appropriate correction function, and transforming back to the time domain. The relevant calibration information is the correction function, which will be generated from the LPF transfer function and a combination of three parameters which need to be specified for each detector: two time constants and their amplitude ratio.

It is also possible to leave this correction to the map-making stage (such corrections can be implemented by MADMAP). If that option is chosen, then this module can easily be by-passed or implemented such that no correction is actually done.

4.1.8 Calculation of source flux density

Let $\mathbf{Q_S}$ be the final vector of signal power timelines after all of the steps above have been implemented. These timelines are to be converted to in-beam source flux density (Jy/beam) as follows.

For a particular detector, let $S_S(n)$ be the in-beam flux density of the source at the telescope aperture.

Q_S for that detector is given by

$$Q_S = A_{\text{Tel}} \int_{\textit{Passband}} S_S(n) h(n)\, \mathrm{d}n \quad , \tag{35}$$

where $A_{\rm Tel}$ is the effective telescope area and $h(\nu)$ is a function representing the overall combination of various efficiencies in the telescope and instrument (obscuration, filters, optics, detector absorption, etc.). If we normalise the product of telescope area and $h(\nu)$ in terms of the relative spectral response function (RSRF), $R(\nu)$ and some calibration constant B, such that

$$A_{\rm Tel} h(\nu) = \frac{R(\nu)}{B} , \tag{36}$$

then

$$Q_{\rm S} = \frac{1}{B} \int_{Passband} S_{\rm S}(\nu) R(\nu) \, {\rm d}\nu . \tag{37}$$

The automatic pipeline must make no assumptions concerning the source spectrum – this is something to be decided upon by the observer, or derived subsequently from a multi-wavelength data-set (SPIRE only or SPIRE plus other measurements such as PACS and/or ground-based observations). Therefore at this stage we must assume a standard spectral form for the source. The simplest approach is to assume that the spectrum is a power law across the band defined by an index $\alpha_{\rm S}$:

$$S_{\rm S}(\nu) = S_{\rm S}(\nu_{\rm o}) \left(\frac{\nu}{\nu_{\rm o}} \right)^{\alpha_{\rm S}} , \tag{38}$$

where we can choose $\nu_{\rm o}$ to be some suitable frequency within the band - for instance at or near the band centres (250, 350, 500 μm) for the three photometer bands.

Typical values for $\alpha_{\rm S}$ would be 2 for a black body in the Rayleigh-Jeans region, 3 - 4 for a dust source in the Rayleigh-Jeans region, or close to 0 for a flat-spectrum radio source or a thermal source observed near the peak of its Spectral Energy Distribution (SED). A wide range of values of α can therefore be expected for SPIRE observations of various kinds.

The signal power is then

$$Q_{\rm S} = \frac{S_{\rm S}(\nu_{\rm o})}{B \nu_{\rm o}^{\alpha_{\rm S}}} \int_{Passband} R(\nu) \nu^{\alpha_{\rm S}} \, {\rm d}\nu , \tag{39}$$

and the source flux density at frequency $\nu_{\rm o}$ is

$$S_{\rm S}(\nu_{\rm o}) = \frac{B Q_{\rm S} \nu_{\rm o}^{\alpha_{\rm S}}}{\int_{Passband} R(\nu) \nu^{\alpha_{\rm S}} \, {\rm d}\nu} = K Q_{\rm S} . \tag{40}$$

The constant K incorporates many factors and is difficult to determine except by observation of a standard astronomical source. Assume that we have such a calibrator with a known spectrum given by

$$S_{\rm C}(\nu) = S_{\rm C}(\nu_{\rm o}) \left(\frac{\nu}{\nu_{\rm o}} \right)^{\alpha_{\rm C}} . \tag{41}$$

For an observation of the calibrator yielding detected power $Q_{\rm C}$, we have

$$S_C(n_o) = B\frac{Q_C n_o^{\,a_C}}{\int_{Passband} R(n)n^{a_C}\,\mathrm{d}n}, \qquad (42)$$

from which we can calculate B:

$$B = \frac{S_C(n_o)\int_{Passband} R(n)n^{a_C}\,\mathrm{d}n}{Q_C n_o^{\,a_C}}, \qquad (43)$$

and K:

$$K = \frac{S_C(n_o)}{Q_C}\left[\frac{n_o^{\,a_S}}{n_o^{\,a_C}}\right]\left[\frac{\int_{Passband} R(n)n^{a_C}\,\mathrm{d}n}{\int_{Passband} R(n)n^{a_S}\,\mathrm{d}n}\right]. \qquad (44)$$

Note that in the idealised case of a top-hat filter and $a_C = 0$, we would have $B = \frac{S_C(n_o)?n}{Q_C}$.

We can now derive $S_S(n_o)$ from an observation of Q_S and an assumed value of a_S. For this we need to know the integrals $\int_{Passband} R(n)n^{a_C}\,dn$ and $\int_{Passband} R(n)n^{a_S}\,dn$ (in the form of calibration files).

Note that accurate knowledge of this integral is not actually critical to the calibration unless the source and calibrator spectral indices are very different, as it tends to ratio out in equation (44):

$$K \approx \frac{S_C(n_o)}{Q_C} \qquad \text{if } a_C \approx a_S\,. \qquad (45)$$

So if the source and calibrator have the same spectral index ($a_S = a_C$), then the expression for the source flux density reduces to a simple ratio as we would expect:

$$S_S(n_o) = S_C(n_o)\left[\frac{Q_S}{Q_C}\right]; \qquad (46)$$

and if we are working in the linear regime in which signal voltage is directly proportional to absorbed signal power, then this further simplifies to

$$S_S(\nu_o) = K V_S = S_C(\nu_o)\left[\frac{V_S}{V_C}\right]. \quad (47)$$

Because the pipeline processing cannot pre-judge the source spectrum, we must assume a standard value of α_S and quote the corresponding flux densities. The observer can then re-calibrate the corresponding flux densities to some other value of α_S if desired.

It is proposed that we adopt $\alpha_S = 0$. It is still possible to derive B from observations of a calibrator with a different spectrum, as long as we know what it is (most of our calibrators are likely to have black or near-black body spectra within a band, for which $\alpha_C = 2$).

We then have a simplified RSRF integral: $\int_{Passband} R(\nu)\, d\nu$, and equation (40) reduces to

$$S_S(\nu_o) = \frac{BQ_S}{\int_{Passband} R(\nu)\, d\nu} = KQ_S \,. \quad (48)$$

In the simple case of a top-hat filter, this would just be $S_S(\nu_o) = \left[\frac{B}{?\,\nu}\right] Q_S$.

The factor K has units Jy W^{-1} and is a suitable calibration quantity with which to characterise the system.
Note that manner in which the normalisation of the RSRF is not critical – it could be done by setting either the peak or the area equal to unity – this would result in different values of B being derived, but the same value for K. We propose that it be normalised such that the peak value is unity.

4.1.9 Conversion of results to a different source spectral index

As discussed above, all results will be calculated and quoted under the assumption that the source has a flat spectrum across the band ($\alpha_S = 0$). This will not be the case in many observations, and a correction will need to be applied by the astronomer based on other information (for instance, measurements in other SPIRE or PACS bands and/or data from other telescopes).
Again, let us assume that the source spectrum actually follows a power law with non-zero index α_S. Let $S'_S(\nu_o)$ be the source flux density at ν_o for that spectral shape. We then have from (35) and (42),

$$S'_S(\nu_o) = S_S(\nu_o)\left[\frac{\nu_o^{\alpha_S} \int_{Passband} R(\nu)\, d\nu}{\int_{Passband} R(\nu)\nu^{\alpha_S}\, d\nu}\right]. \quad (49)$$

The factor in brackets can easily be computed and tabulated for various values of a_S, so that the astronomer can implement a straightforward multiplicative correction factor corresponding to the chosen spectral index.

Note that it is equally straightforward to convert the results to some other wavelength if that is desired. Sometimes it is the practice to quote the measured flux density at a flux-weighted effective wavelength, to take into account the fact that the measurement is biased towards one side of the band in the case of a source with a steep spectrum. We propose not to adopt this practice here for two reasons:

(i) it is no more accurate or correct than the scheme described above;
(ii) we can avoid complication and potential confusion by selecting a standard set of wavelengths for all measurements.

4.1.10 Summary of the model-based pipeline

The basic steps in the model-based pipeline are shown in

Figure 18 and may be summarised as follows:

1. Determine the bolometer voltage, current, resistance timelines
2. Determine the timeline of the bolometer bath temperature
3. Calculate the absorbed radiant power (signal + background)
4. Remove electrical crosstalk
5. Subtract the background:
   - for point source and jiggle-map observations, the background is automatically removed
   - for scan map: use a calibration observation of blank sky to subtract the background
6. Remove optical crosstalk
7. Correct for beam spearing due to scan speed
8. Convert the calculated absorbed signal power to flux density using knowledge of the RSRF, and assumed source spectral index, and observation of a standard astronomical calibrator

All corrections for the effects of temperature drifts, detector bias setting, and detector non-linearity are fully accounted for in this procedure.

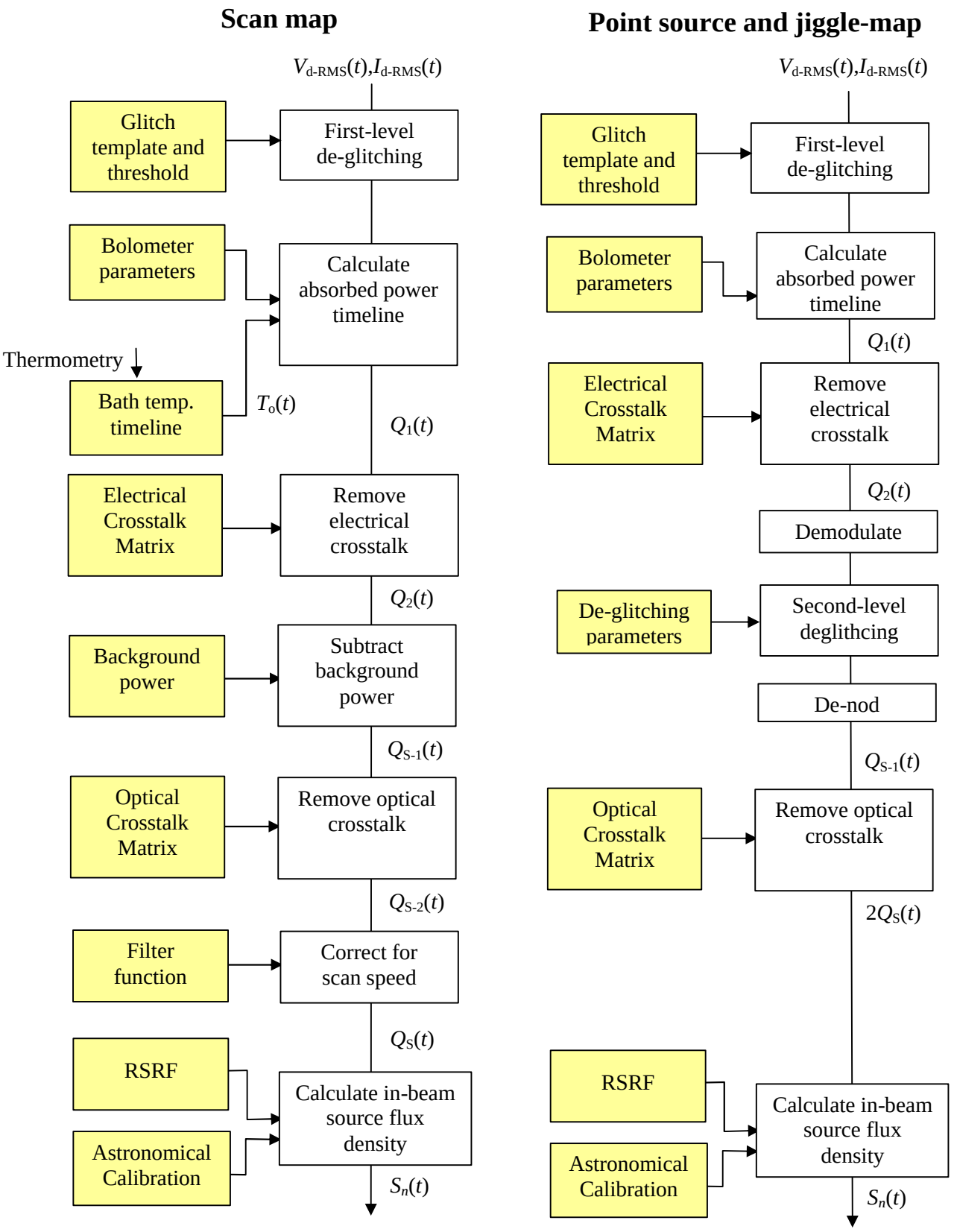

Figure 18: Block diagram of the full photometer pipeline for scan map (left) and point source/jiggle map (right).

4.2 Empirical photometer pipeline

In this section we outline a simplified pipeline based on the use of the detector voltage as a measure of the astronomical flux density.

Let the bolometer RMS output voltage be

$$V_{\mathrm{d-rms}} = V_{\mathrm{o}} + V_{\mathrm{S}}, \tag{50}$$

where V_{o} represents the operating point voltage in the absence of any astronomical signal, and V_{S} is due to the astronomical signal (V_{S} is negative as the bolometer resistance decreases with increasing absorbed power).

V_{o} depends on the bolometer parameters, operating temperature, and bias setting, and on the background power from the telescope. We assume that it is constant to first order throughout the observation. It must be subtracted in order to determine the signal voltage. This is simple in the case of point source and jiggle map observations, less so for scan map (see below).

4.2.1 Removal of electrical crosstalk

Let the value of $V_{\mathrm{d\text{-}RMS}}$ for bolometer I be denoted $V_{\mathrm{1\text{-}I}}$. The procedure for removing electrical crosstalk is identical to that for the model-based pipeline (Section 4.1.4), except that we use the measured bolometer voltages, $V_{\mathrm{1\text{-}i}}$, rather than the absorbed radiant powers. The vector of electrical crosstalk-corrected signals is given by

$$\mathbf{V_2} = \mathbf{C_{elec}}\,\mathbf{V_1}. \tag{51}$$

4.2.2 Removal of correlated noise due to temperature fluctuations (scan-map only)

Recall that in the model-based pipeline, these fluctuations are to be removed via direct tracking of the bath temperature. This cannot be done in the empirical pipeline, but there are two other options:

1. use of the correlations between the detector outputs themselves;
2. use of the correlations between the detectors and the array thermometers or blind pixels.

For Option 1, the procedure is as follows:

- take the median signal timeline of all the detectors in an array (or perhaps a set of them around the periphery of a "source" – but that has to be done at the level of the map rather than the timeline);
- adjust the median timeline so that its mean is zero;
- subtract this from each individual detector timeline

This method will not introduce much additional noise as the timeline to be subtracted is averaged over many detectors. However, there are two problems with this method: firstly, for scanning observations, large-scale sky structure can mimic bath temperature fluctuations (all the detectors going up and down together) and so can be removed by this process; secondly, the presence of strong emission in a part of the map will bias median timeline, resulting in potential removal of some real signal.

Option 2 is similar in principle to the use of an independent $T_{\mathrm{o}}(t)$ timeline in the model-based pipeline. A voltage timeline $V_{\mathrm{th}}(t)$ is generated for each detector by a TBD algorithm using the array thermometers and/or blind pixels. This is then subtracted from that detector's signal timeline. The thermometer signals must be averaged over a period of time to reduce the noise level, and thermal fluctuations on shorter timescales will not be tracked.

In order to have a scheme that does not involve potential loss or distortion of the astronomical signal, and one which is similar to the model-based pipeline version, Option 2 is to be adopted as the baseline.

Following these two steps (DC offset and correlated noise removal), the detector signal timelines are converted to source flux density.

4.2.3 DC offset (V_o) removal

Point source and jiggle-map observations: For observations involving chopping and nodding, V_o is removed automatically as the demodulated nod signal is proportional to V_S following the treatment of Section 4.1.5, but working now with voltage rather than absorbed power).

Scan-map observations: We propose a procedure essentially the same as that for removing the telescope background power for the model-based pipeline. Standard calibration observations are carried out of "dark" areas of sky to produce a calibration file corresponding to the detector operating point voltage under the nominal conditions ("dark sky", known telescope and Level-1 temperatures).

A TBD algorithm is then implemented, which uses these calibration files and makes any small corrections for different telescope and L-1 temperatures to calculate V_o for each detector for the particular conditions applying to the observation (as for the model-based pipeline).

The signal power timelines (V_S) can then be calculated by subtracting this from the measured timeline V.

4.2.4 Removal of optical crosstalk

Let V_{S1} be the detector voltage after DC offset removal. The procedure for removing optical crosstalk is identical to that for the model-based pipeline (Section 4.1.6). The vector of optical crosstalk-corrected signals is given by

$$\mathbf{V_{S2}} = \mathbf{C_{opt}}\,\mathbf{V_{S1}}\,. \tag{52}$$

The optical crosstalk matrix, $\mathbf{C_{opt}}$, can be implemented as a calibration file whose elements, o_{ij}, must be determined from calibration observations involving scanning a strong point source across each of the detectors in the array.

4.2.5 Correction for beam smearing due to scan speed (scan-map only)

This can be implemented in a manner similar to the case of the model-based pipeline, the only difference being that the operation is carried out on the voltage timeline rather than a signal power timeline.

4.2.6 Derivation of source flux density and detector non-linearity correction

Let $\boldsymbol{V_S}$ be the final vector of signal voltage timelines after all of the steps above have been implemented. The calculation of source flux density can follow the procedure of Section 4.1.8 except that Q is replaced by V and the constant K now has units of Jy V^{-1} instead of Jy W^{-1}.

Two adjustments which are automatically taken into account in the model-based pipeline must be explicitly implemented here:

(i) correction for detector non-linearity when observing strong sources;
(ii) correction for any drifts in detector responsivity.

Strong source correction: For small signals, V_S is proportional to the in-beam source flux density (equation 47):

$$S_S(n_o) = K V_S\,. \tag{53}$$

For very strong sources, the relationship between voltage and flux density ceases to be linear. Two methods of correction for this non-linear bolometer response to strong sources are considered.

Option 1: The bolometer response as a function of source strength can be represented by a low-order polynomial function. A second-order polynomial is adequate to account for the non-linear response for signal levels comparable to or greater than the telescope background [5]. We can therefore characterise the relationship between signal voltage and source flux density as follows:

$$S_S(\nu_o) = KV_S + K_1 V_S^{\,2} \,. \tag{54}$$

The constants K and K_1 can be incorporated into calibration files, with K determined (following equation 44) from observations of an astronomical calibration source of moderate brightness. K_1 can be found by observing the departure from linearity for a strong source of known brightness (or from the standard bolometer model, if such a source is not available). Both K and K_1 are specific to a particular detector bias setting

Option 2: For an NTD bolometer with a given applied bias voltage, the small-signal responsivity varies with the voltage across the bolometer with an approximately linear relationship over a wide range background loading conditions [5]. This translates to a corresponding relationship for the differential sensitivity of the system to astronomical source flux density:

$$\frac{dV_{\text{d-RMS}}}{dQ} \propto V_d \quad \Rightarrow \quad \frac{dV_{\text{d-RMS}}}{dS_S} \propto V_{\text{d-RMS}} \,. \tag{55}$$

Let

$$\frac{dS_S}{dV_{\text{d-RMS}}} = f(V_{\text{d-RMS}}), \tag{56}$$

where we allow for the possibility that $f(V_{\text{d-RMS}})$ may actually depart form linearity. For the case of blank sky (negligible astronomical power), we have $K = f(V_o)$.

The function $f(V_{\text{d-RMS}})$ is specific to a particular bias setting, and can be determined by pointing the telescope at a selection of bright sources (without chopping) and measuring the relative change in responsivity as a function of bolometer voltage using PCal. Except for one primary calibrator, it is not necessary to know how bright the sources are – they are just being used to establish a range of backgrounds on the detectors.

To calibrate observations of strong sources, the flux density can be determined by integrating the above expression between the off source (blank-sky) RMS detector voltage, V_o, and the RMS detector voltage when observing the source, V_{so}:

$$S = \int_{V_o}^{V_{so}} f(V_{\text{d-RMS}})\, dV_{\text{d-RMS}} \,. \tag{57}$$

Option 2 is preferred as it has the advantages that only one astronomical calibrator is needed, and that the characterisation of the responsivity as a function of operating point voltage using PCal is not model-dependent. The signal from a faint source observed with a certain operating point voltage can also be converted to any other operating point voltage.

Note:

(a) For either method, the constants K and K_1 or the function $f(V)$ will also have some dependence on the detector bath temperature, T_o, and the total background power. These dependencies are small and can be computed using the bolometer model. They could be incorporated into equations (55) or (56) by establishing the calibration files for the nominal conditions and modifying them according to a simple algorithm that takes the telescope, instrument and ^{3}He temperatures into account.

(b) If $f(V)$ is a linear function, then

$$S = \int_{V_o}^{V_{so}} \left(mV_{\mathrm{d-RMS}} + K \right) \mathrm{d}V_{\mathrm{d-RMS}} \ , \tag{58}$$

where m and K are constants, so

$$S = \frac{m}{2}\left({V_{so}}^2 - {V_o}^2 \right) + K\left(V_{so} - V_o \right) , \tag{59}$$

which we can write as

$$S = K\left(V_{so} - V_o \right) + K_1\left({V_{so}}^2 - {V_o}^2 \right) . \tag{60}$$

Here $V_{so} - V_o$ is equivalent to V_S as defined above, so K has the same definition; but K_1 now has a slightly different definition, being applied to ${V_{so}}^2 - {V_o}^2$ rather than $(V_{so} - V_o)^2 = {V_{so}}^2 + {V_o}^2 - 2V_{so}V_o$.

Responsivity drift correction (small-signal case only): The baseline option is to use the bolometer operating point voltage to track the small signal responsivity, using equation 56, so the operating point voltage can also be used to apply a correction to the nominal value of K: $K = f\left(V_o \right)$.

Note: Changes to the nominal value of K are also tracked using the regular PCal measurements (which are nominally made off-source) both before and after the observation. An alternative approach would be to use PCal data may be analysed to derive the timeline, $\gamma(t)$, of relative changes in K, such that

$$K(t) = g(t)K_{\mathrm{nom}} . \tag{61}$$

These PCal measurements during AOTs will be used in any case for trend analysis, and a pipeline module allowing the option of incorporating this option will be retained.

4.2.7 Summary of the empirical pipeline

The basic steps in the empirical pipeline are as follows:

1. Determine the bolometer voltage timeline (DC offset + signal timeline).
2. Remove electrical crosstalk.

3. For scan map observations, remove correlated noise by subtracting a timeline derived, using a TBD algorithm, from the array thermometers and/or blind detectors.
4. Subtract the DC offset
   - for point source and jiggle-map observations, the offset is automatically removed;
   - for scan map: use a calibration observation of blank sky to subtract the offset.
5. Remove optical crosstalk.
6. Correct for beam smearing due to scan speed.
7. Convert the signal voltage to source flux density (incorporating a correction factor for any detector non-linearity) using:
   - characterisation of the relative small-signal responsivity as a function of operating point voltage;
   - knowledge of the RSRF;
   - an assumed source spectral index;
   - observations of standard astronomical calibrators;

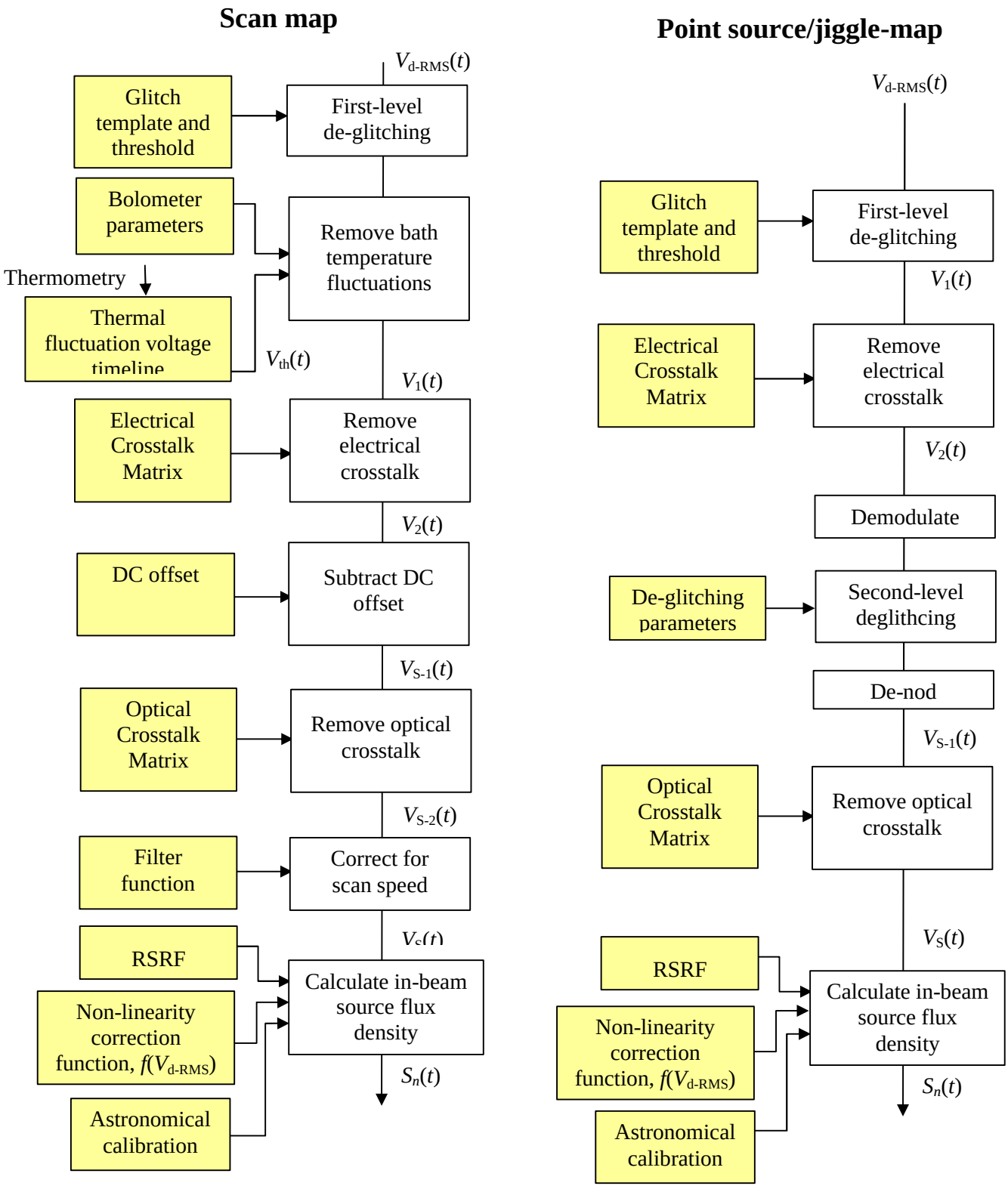

Figure 19: Empirical photometer pipeline block diagram for scan map (left) and point source/jiggle map (right).

4.2.8 Comparison of the two pipeline approaches

Calculation of bolometer electrical parameters from the telemetry: This is the same for both.

Removal of T_0 fluctuations: In each case a timeline is derived from the thermometers and used to correct the detector timelines. In the case of the empirical pipeline, the correction is empirical, based on some calibration measurements. The model-based pipeline needs accurate thermometry and knowledge of the bolometer model parameters have to be well known, so it could be more difficult to implement.

Removal of bolometer non-linear response: The model-based pipeline again relies on the bolometer model and good knowledge of the relevant parameters. In the case of the empirical pipeline, the correction is implemented in an empirical procedure that can be derived from one calibration source and characterisation of the bolometer small signal responsivity vs. operating point voltage.

Removal of bolometer responsivity drifts: This is not needed in the model-based pipeline, and is carried out using PCal data (or monitoring of the operating point) in the empirical pipeline.

Conclusions

1. The empirical pipeline should be implemented in the first instance as it is based on established and proven methods, and does not require use of the bolometer model.

2. The pipeline architecture should be made as compatible as possible with a future upgrade to the model-based pipeline.

5. References

1 *DCU Design Document*, SA-SPIRE-FP-0063-02, Issue 1.0, 11 July 2005.

2 *SPIRE spectrometer pipeline description*, SPIRE-BSS-DOC-002966, Version 1.5, 2 October 2007.

3 Mather, J C. Bolometer noise: nonequilibrium theory. *Applied Optics* 21, 1125, 1982

4 Sudiwala, R V, M J Griffin, and A L Woodcraft. *Thermal modelling and characterisation of semiconductor bolometers*. Int. J. Infrared. Mm. Waves, 23, 575, 2002.

5 *Sensitivity of the SPIRE Detectors to Operating Parameters*, SPIRE-UCF-DOC-002901, Issue 1.0, June 7 2007.